A THESIS

on

SYNTHESIS AND CHARACTERIZATION OF CdS/SiO_2 CORE/SHELL NANOPARTICLES DOPED WITH SILVER

Submitted in the partial fulfillment of requirement for the award of the Degree of

Master of Science (PHYSICS)

Submitted by:

MANVEEN KAUR

Roll No.: 30704009

Under the Guidance of

Dr. N.K.VERMA

Professor and Dean

School of Physics and Materials Science

THAPAR UNIVERSITY

PATIALA (PUNJAB)-147 004

JULY 2009

Dedicated

To

My Parents

CERTIFICATE

This is to certify that the report entitled "**Synthesis and characterization of CdS/SiO_2 core/shell nanoparticles doped with silver**" submitted by **Manveen Kaur, Roll No. 30704009**, student of M.Sc (Physics), Thapar University, Patiala, was carried out by her under my supervision. She has not submitted this material for credit towards any other degree at Thapar University, Patiala or any other University.

13/7/09

(N. K. Verma)
Supervisor
Professor and Dean
School of Physics & Materials Science
Thapar University
Patiala

(O. P. Pandey)
Professor and Head
School of Physics & Materials Science
Thapar University
Patiala

R K Sharma 13/7/09

(R. K. Sharma)
Dean of Academic Affairs
Thapar University
Patiala

ACKNOWLEDGEMENT

I may halt for a while and avail this opportunity to place on record my gratefulness to all those, who have made a direct or indirect contribution towards the successful completion of this thesis. Above all, I express my gratitude to the **Almighty** for his grace and blessings.

With deep sense of gratitude I express my sincere thanks to my esteemed and worthy supervisor **Dr. N. K. Verma**, Professor, School of Physics, for his valuable guidance in carrying out this work under his effective supervision, encouragement, enlightenment and cooperation.

My special thanks to **Ms. Zinki Jindal**, **Mr. Sanjeev Kumar** and **Mr. Sunil Kumar**, for their timely help, cooperation and useful discussions.

I owe my sincere thanks to all the staff members of School of Physics and Materials Science for their support and encouragement.

The work is incomplete without paying regards to my respected parents whose blessings and encouragement have shown me the path to pursue goals in my life.

Manveen Kaur

(Manveen Kaur)

Abstract

CdS is a II-VI, direct band gap semiconductor having interesting optoelectronic properties such as photocatalytic and nonlinear optical properties. CdS/SiO_2 core/shell nanoparticles have improved applications due to the surface modification of CdS nanoparticles. The mesoporous silica shell of the nanocomposites also plays a key role in the process of fluorescence enhancement, which helps to protect the surface characteristics of QDs, prevent the flocculation of the particles. CdS/SiO_2 core/shell nanoparticles doped with silver have been synthesized via the sol-gel technique using hydrolysis of tetraethyl orthosilicate (TEOS). Based on the method, five samples with different concentrations of $AgNO_3$ have been synthesized. The crystal structure and the average crystallite size of the samples have been calculated using X-ray diffraction studies. The elemental analysis has been carried out by EDAX spectroscopy and FTIR spectroscopy. The band gap of CdS/SiO_2 core/shell nanoparticles has been calculated by UV-Visible absorption spectra. Room temperature PL studies have been carried out to study the emission characteristics of the synthesized nanoparticles.

Contents

CHAPTER 1

INTRODUCTION

1.1 Introduction to Nanoscience and Nanotechnology

Nanotechnology is the technology which uses phenomena and structures that can only occur at the nanometer scale, which is the scale of single atoms and small molecules. Nanotechnology is the understanding and control of matter at dimensions of roughly 1 to 100 nanometer, where unique phenomena enable novel applications.

The related term nanoscience is used to describe the interdisciplinary fields of science devoted to the study of nanoscale phenomena employed in nanotechnology. This is the world of atoms, molecules, macromolecules, quantum dots, and macromolecular assemblies, and is dominated by surface effects such as van der Waals force of attraction, hydrogen bonding, electronic charge, ionic bonding, covalent bonding, hydrophobicity, hydrophilicity, and quantum mechanical tunneling, to the virtual exclusion of macro-scale effects such as turbulence and inertia. For example, the vastly increased ratio of surface area to volume opens new possibilities in surface-based science, such as catalysis.

1.2 History

The first mention of some of the distinguishing concepts in **nanotechnology** was in "There's Plenty of Room at the Bottom", a talk given by Richard Feynman at an American Physical Society meeting Caltech on December 29, 1959. Feynman described a process by which the ability to manipulate individual atoms and molecules might be developed, using one set of precise tools to build and operate another proportionally smaller set, so on down to the needed scale. In the course of this, he noted, scaling issues would arise from the changing magnitude of various physical phenomena: gravity would become less important, surface tension and van der Waals attraction would become more important, etc.

The term "nanotechnology" was defined by Tokyo Science University Professor Norio Taniguchi in a 1974 paper as follows: “Nanotechnology mainly consists of the processing, separation, consolidation, and deformation of materials by one atom or one molecule." In the 1980s the basic idea of this definition was explored in much more depth by Dr. Eric Drexler, who promoted the technological significance of nanoscale phenomena and devices through speeches and the books "Engines of Creation: The Coming Era of

Nanotechnology" and "Nanosystems: Molecular Machinery, Manufacturing, and Computation", and so the term acquired its current sense.

More broadly, nanotechnology includes the many techniques used to create structures at a size scale below 100 nm, including those used for fabrication of nanowires, those used in semiconductor fabrication such as deep ultraviolet lithography, electron beam lithography, focused ion beam machining, atomic layer deposition, and molecular vapor deposition, and further including molecular self-assembly techniques.

1.3 Unique Properties at Nanoscale

Four important ways in which nanoscale materials may differ from macroscale materials are as follows:

- Gravitational forces become negligible and electromagnetic forces dominate
- Quantum mechanics model is used to describe motion and energy instead of the classical mechanics model
- Greater surface area to volume ratio
- Random molecular motion becomes more important

These can affect the optical, electrical and magnetic behavior of materials, particularly as the structure or particle size approaches the smaller end of the nanoscale. Materials that exploit these effects include quantum dots, and quantum well lasers for optoelectronics.

1.3.1 Optical properties

The optical properties of a material result from the interaction of light with the composition and atomic structure of the material. Color, luster, and fluorescence are examples of well-known optical properties. At the nanoscale, some interesting optical properties emerge. Gold nanoparticles and zinc oxide are interesting examples. These substances exhibit different properties as bulk samples compared to nanosized samples. Bulk gold is yellow in colour while nanosized sample is red in colour. Bulk Zinc oxide (ZnO) is white in colour while nanosized particle of ZnO is transparent. The underlying principle governing the color changes between a bulk sample and a nano can be explained as follows: When light is shone on a piece of metal, the photons strike the electrons in the metal. In bulk metal,

electrons are free to move more or less randomly throughout the crystal structure of the metal. However, in a very thin film of metal lying upon an insulator (such as glass), the electrons are confined to a thin region. When the light strikes on these electrons the electrons will move in a coherent wave, rather than being free to move randomly. These coherent waves of electrons are called surface plasmons. The size of these waves of electrons depends upon the thickness of the film. If an incoming photon has just the right wavelength, its energy will be completely absorbed by the metal, and turned into a surface plasmon. This is called surface plasmon resonance, i.e. the incoming photon resonates with the kind of electron waves produced in the film. Photons that do not resonate with the metal film will be reflected back. Consequently when white light strikes upon such a metal film, the film selectively absorbs photons at a certain small range of wavelengths.

Another factor is larger surface area/volume ratio. Since the nanoparticles have dominating surface, the Surface Plasmon Resonance (SPR) effect takes place.

1.3.2 Chemical reactivity

Just as changes in the optical and electronic properties of nanoscale materials are anticipated based on quantum confinement effects, changes in chemical reactivity of nanoscale materials have also been anticipated. As chemical reactions are governed by electrons, relative electron affinities or ionization potentials, and electron orbital densities, a natural coupling exists between chemical reactivity and the electronic character of the reactants and any reaction catalysts. In transition metal atom clusters, ionization potential increases as the cluster size drops below the bulk limit. The increase in ionization potential does not, however, always vary monotonically with cluster size. Nanoparticles can also be arranged into layers on surfaces, providing a large surface area and hence enhanced activity, relevant to a range of potential applications such as catalysts.

1.3.3 Mechanical strength

For materials such as crystalline solids, as the size of their structural components decreases, interface area becomes greater; which can greatly affect both mechanical and electrical properties. For example, most metals are made up of small crystalline grains; the boundaries between the grain slow down or arrest the propagation of defects when the material is stressed, thus giving it strength. If these grains can be made very small, or even nanoscale in size, the interface area within the material greatly increases, which enhances its strength. For example, nanocrystalline nickel is as strong as hardened steel.

1.3.4 Melting point

Melting Point is the temperature at which the atoms, ions, or molecules in a substance have enough energy to overcome the intermolecular forces that hold them in a fixed position in a solid. At nanoscale, surface atoms require less energy to move because they are in contact with fewer atoms of the substance.

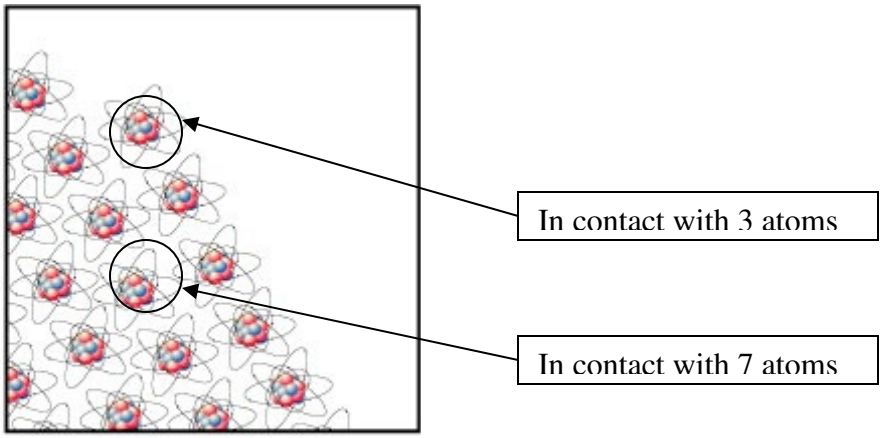

Figure 1.1: At nanoscale, surface atoms are in contact with fewer atoms as compared to inner atoms.

1.4 Quantum Confinement

Nanotechnology has yielded a number of unique structures that are not found anywhere in nature. Most demonstrate an essential quality of quantum mechanics known as quantum confinement. The idea behind confinement is all about keeping electrons trapped in a small

area. The sizes for confinement have to be less than 30 nm for effective confinement. Quantum confinement comes in several flavors. 2-D confinement is only restricted in one dimension, and the result is a quantum well (or plane). These are what most lasers are currently built from. 1-D confinement occurs in nanowires. 0-D confinement is found only in the quantum dot.

Confinement is important as it leads to new electronic properties that are not present in bulk semiconductor devices. The typical quantum dot is anywhere between 3-60 nm in diameter. That is still 30 to 600 times the size of a typical atom. Quantum dots are large enough to be manipulated by magnetic fields and can even be moved around with an STM or AFM. Many important atomistic characteristics can be deduced from a quantum dot that would otherwise be impossible to research in an atom.

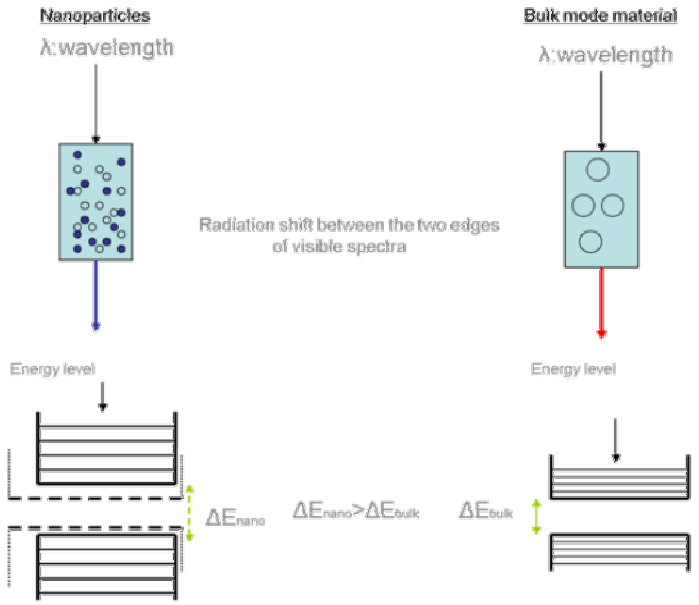

Figure 1.2: Figure illustrating that quantum confinement is responsible for the increase of energy difference between energy states and band gap.

Quantum confinement is responsible for the increase of energy difference between energy states and band gap. A phenomenon tightly related with the optical and electronic properties of the materials. The quantum confinement effect can be observed once the

diameter of the particle is of the magnitude as the wavelength of electron wave function [1]. When the materials are so small, their electronic and optical properties deviate substantially from those of bulk materials [2].

A particle behaves as if it were free when the confining dimension is large compared to the wavelength of the particle. During this state, bandgap remains at its original energy due to continuous energy state. However, as the confining dimension decreases and reaches a certain limit, typically in nanoscale, the energy spectrum turns to discrete. As a result, bandgap becomes size dependent. This ultimately results a blue shift in optical illumination as the size of the particles decreases.

Specifically, the effect describes the phenomenon results from electrons and electron holes being squeezed into a dimension that approaches a critical quantum measurement, called the exciton Bohr radius. Nanocrystals lie in between the atomic and the molecular limit of discrete density of electronic states and the extended crystalline limit of continuous band [3].

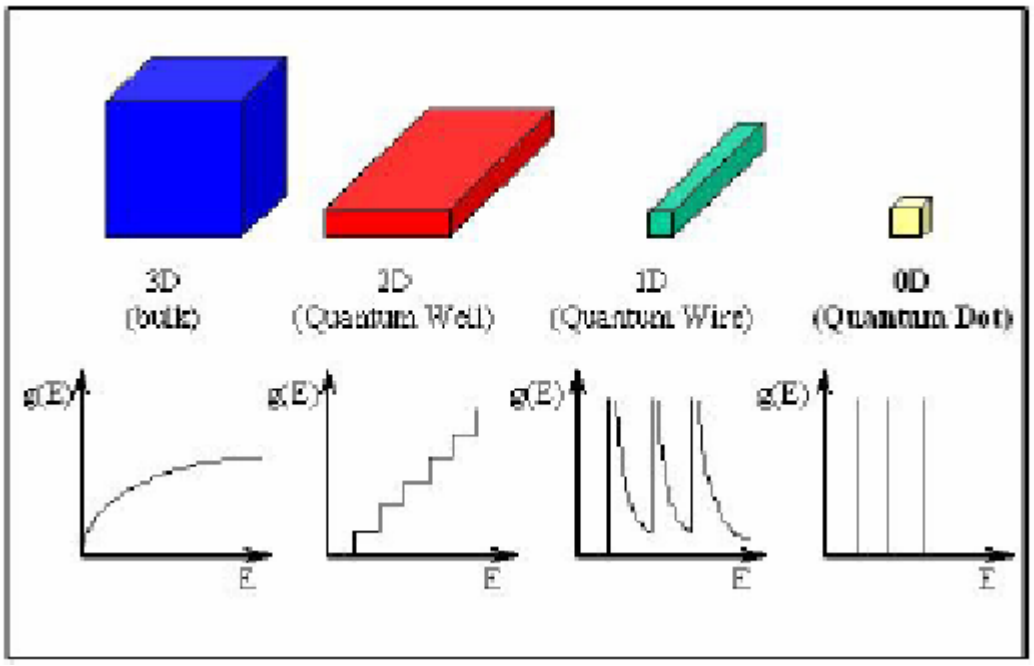

Figure 1.3: Evolution of the density of the states as the dimensionality of the structure is reduced from the 3D (bulk) to 0D (quantum dot). The density of the states of an ideal quantum dot is discrete, like an atom.

1.5 Exciton

An exciton is a bound state of an electron and an imaginary particle called an electron hole in an insulator (or semiconductor), or in other words, a Coulomb correlated electron-hole pair. It is an elementary excitation, or a quasiparticle of a solid.

A vivid picture of exciton formation is as follows: a photon enters a semiconductor, exciting an electron from the valence band into the conduction band. The missing electron in the valence band leaves a hole behind, of opposite electric charge, to which it is attracted by the Coulomb`s force. Exciton results from the binding of the electron with its hole; as a result, the exciton has slightly less energy than the unbound electron and hole. The wavefunction of the bound state is hydrogenic i.e. an "exotic atom" state akin to that of a hydrogen atom. However, the binding energy is much smaller and the size much bigger than a hydrogen atom because of the effects of screening and the effective mass of the constituents in the material. Excitons are thus, the main mechanism for light emission in semiconductors at low temperatures being less than the exciton binding energy, replacing the free electron-hole recombination at higher temperatures.

1.6 Surface to Volume Ratio

As surface area to volume ratio increases**,** a greater amount of a substance comes in contact with surrounding material. This results in better catalysts, since a greater proportion of the material is exposed for potential reaction.

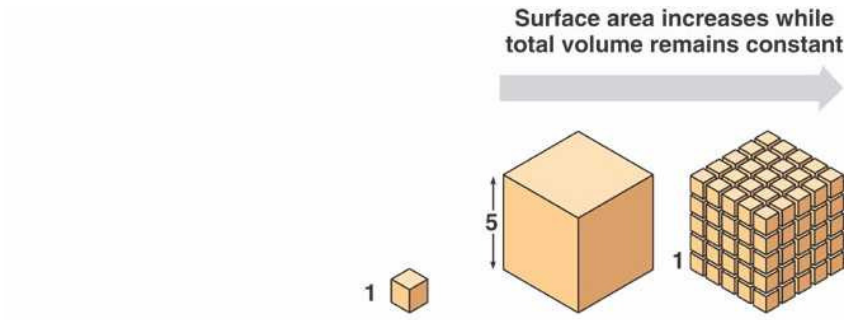

Total surface area (height × width × number of sides × number of boxes)	6	150	750
Total volume (height × width × length × number of boxes)	1	125	125
Surface-to-volume ratio (surface area / volume)	6	1.2	6

Figure 1.4: Figure illustrates that surface to volume ratio increases at small scale

1.7 Methods of fabrication

In general, there are two philosophically distinct approaches for making nanostructures, which can be characterized as top-down and bottom-up.

Top-down approach begins with larger starting materials and, in a more or less controlled fashion, removes the material until the desired structure is achieved. In this approach, small features are patterned in bulk materials by a combination of lithography, etching and deposition to form functional devices. Most microfabrication techniques for inorganic materials such as lithography and milling fit this description. Production processes by using top-down approach are:

- High energy milling
- Chemical mechanical milling
- Vapor phase condensation
- Electro-explosion
- Laser ablation

- Sputtering

In contrast, **bottom-up approach** begins with smaller subunits that are assembled, with varying levels of control, depending on technique, into the final product. Key examples of materials made by bottom-up approaches include some inorganic structures. This includes structures created by using direct atomic or molecular placement by force microscopy; structures built using various deposition or growth methods, as well as polymerization methods of synthesis. Production processes by using bottom-up approach are:

- Crystallisation
- Sol-gel
- Chemical vapour deposition
- Solvothermal/Hydrothermal
- Micelle and micro emulsion synthesis
- Spray pyrolysis
- Template Synthesis: Electrochemical and Electroless

1.8 Literature review

Semiconductor nanoparticles have attracted great interest in both theoretical research and technological applications [5]. Size-selective photoetching technique as a means of preparing monodisperse semiconductor nanoparticles has been developed by Tsukasa. With irradiation of monochromatic light, the diffuse reflectance spectra of silica-coated CdS nanoparticles were blue-shifted, and finally the absorption onset matched well with the wavelength of irradiation light [6]. CdS-capped SnO_2 (CdS@SnO_2) and SiO_2 (CdS@SiO_2) colloids of 50-80 Å in diameter have been prepared in aqueous medium. Significant quenching of CdS emission is observed in the CdS@SnO_2 system as the electrons are injected from the excited CdS shell into the SnO_2 core [7]. Aslan et al. developed core-shell (silver core-silica shell) nanoparticles with various shell thicknesses featuring a variety of fluorophores, to show the versatility of the core-shell architecture, and have demonstrated their applicability for two platform technologies, metal-enhanced fluorescence (MEF) and single nanoparticles sensing [8]. Development of spherical Ag@SiO_2 nanocomposites in which fluorescein isothiocyanate molecules have been incorporated using a silane coupling

agent and a straightforward microemulsion-based synthesis procedure has been reported by M. L. Viger. The photophysical characteristics of core-shell and coreless nanostructures with similar silica shell thickness and fluorophore densities are measured and compared, and show unequivocally that the presence of the silver core decreases the fluorophore lifetime by a factor as high as 4 and that the steady-state fluorescence intensity is increased by a factor as high as 3. The relationship between the enhancement in fluorescence yield and the influence of the silver core on resonance energy transfer processes was examined by fluorescence lifetime and anisotropy measurements. These $Ag@SiO_2$ core-shell nanoparticles provide higher detectability and lower self-quenching, whereas the faster recycling time offers more robustness toward photobleaching [9]. In another work monodispersed $CdS–SiO_2$ core-shell particles ranging from nanometers (30–100 nm) to micrometers (1.5–2 μm) were prepared in situ in the nonionic reverse microemulsions. After treating the core-shell particles with concentric nitric acid, the hollow silica spheres were obtained correspondingly [10]. Monodispersed CdS nanoballs were synthesized through γ-irradiating $CdCl_2$, $Na_2S_2O_3$ and polyvinylpyrrolidone aqueous solution at room temperature. With these well monodispersed CdS nanoballs, $CdS@SiO_2$ core–shell structures were prepared under hydrolysis of tetraethylorthosilicate without adding a coupling agent [11]. CdS/Silica core/shell nanoparticles have been synthesized by directly covering silica on the CdS nanocrystalline surface in the same reverse microemulsion composed of polyoxyethylene (10) tertoctylphenyl ether (Triton X-100)/1-hexanol/cyclohexane/H_2O [12]. In a study, the high-intensity ultrasound was applied in the preparation of chiral polyurethane/$CdS–SiO_2$ nanocomposites [13]. CdS/silica xerogel glasses were prepared via silica gels containing mixture solution of 0.2 M ($CdCl_2$ and thiourea) with molar ratio 1:1 [14]. Mn-doped CdS nanocrystals were synthesized via the modified reverse-micelle method and then a CdS/SiO_2 core–shell structure was prepared under hydrolysis of tetraethyl orthosilicate (TEOS) without any coupling agent [15]. Several different combinations of core/shell nanoparticles, such as CdSe/ZnS [16, 19], CdS/ZnS [20-23], CdSe/CdS [17, 18], CdS/PbS [24], CdS/HgS [25], and CdS/Ag_2S [26, 27] have been synthesized and studied for their photoluminescence properties. However, CdS/SiO_2 core/shell nanoparticles doped with silver have not been reported yet as per the best of our knowledge.

CHAPTER 2

MATERIALS AND CHARACTERIZATION

2.1 Cadmium Sulfide (CdS)

The II-VI compound semiconductors like, Cadmium selenide (CdSe), Cadmium sulfide (CdS), Cadmium telluride (CdTe), Zinc oxide (ZnO), Zinc selenide (ZnSe), Zinc sulfide (ZnS) and Zinc telluride (ZnTe) have been the subject of extensive research both in fundamental studies and for potential applications in devices. The broad range of band gap and lattice constants available from these materials, and the unique fundamental phenomena they exhibit make them attractive for a wide range of applications such as infrared lasers and detectors, blue-green lasers and light emitting diodes (LEDs), nonlinear optical materials, magneto-optical devices and radiation detectors.

Cadmium sulfide is a chemical compound with the formula CdS. It is a yellow colored semiconductor [28], existing as two different minerals, the more stable hexagonal wurtzite structure (found in the mineral Greenockite) and the cubic zinc blende structure (found in the mineral Hawleyite) [29]. In both of these forms the Cadmium and sulfur atoms are four coordinate. It is a direct band gap semiconductor (2.42 eV) [30] and has many applications for example in light detectors. It forms thermally stable pigments and with the addition of materials like CdTe and HgS, colors ranging from deep red to yellow are formed [31].

(a) **(b)**

Figure 2.1 (a) 3D model of the structure of hawleyite. (b) 3D model of the structure of greenockite

Cadmium sulfide can be prepared by the precipitation from soluble cadmium (II) salts with sulfide ion and this has been used in the past for the gravimetric analysis of cadmium.

$$Cd^{2+} + NH_3 \rightarrow [Cd\ (NH_3)_4]^{2+} \qquad (2.1)$$

Pigment production usually involves the precipitation of CdS, the washing of the precipitate to remove soluble cadmium salts followed by calcination (roasting) to convert it to the hexagonal form followed by milling to produce a powder. The preparative route and the subsequent treatment of the product, affects the polymorphic form that is produced. It has been asserted in the past that chemical precipitation methods produce the cubic zinc blende form however there more recent examples where the hexagonal form is produced, e.g. see [32].

Cadmium sulfide is soluble in acids and this has been investigated as a method of extracting the pigment from waste polymers e.g. HDPE pipes: [33]

$$CdS + HCl \rightarrow CdCl_2 + H_2S \qquad (2.2)$$

When sulfide solutions containing dispersed CdS particles are irradiated with light hydrogen gas is generated: [34]

$$H_2S \rightarrow H_2 + S\ ;\ \Delta H_f = +9.4\ \text{kcal/mol} \qquad (2.3)$$

The reaction mechanism proposed involves the electron/hole pairs created when incident light is absorbed by the cadmium sulfide followed by these reacting with water and sulfide [35]. Some other properties of CdS have been listed as follows:

- the conductivity increases when irradiated with light (leading to uses as a photoresistor)
- when combined with a p-type semiconductor it forms the core component of a photovoltaic (solar) cell and a CdS/Cu_2S solar cell was one of the first efficient cells to be reported (1954) [36, 37]
- when doped with for example Cu^+ ("activator")and Al^{3+} ("coactivator") CdS luminesces under electron beam excitation (cathodoluminescence) and is used as phosphor
- both polymorphs are piezoelectric and the hexagonal is also pyroelectric

- electroluminescence
- solid CdS can act as a solid state laser

2.2 Silver (Ag) Dopant

Silver is a chemical element with the chemical symbol Ag and atomic number 47. Ag is a soft, white, lustrous transition metal, having the highest electrical conductivity of any element and the highest thermal conductivity of any metal.

There is a growing literature on the optical and electronic properties and uses of silver nanostructures, particularly silver colloids [38, 39]. These display bright colors due to the plasmon absorption, which is due to a combination of both absorption and scatter [40, 41]. The control of the nanoscale optical properties of silver nanostructures has led to nanophotonic devices ranging from nanosensors [42] to waveguides [43], as well as in a wide variety of applications in biotechnology [44-48]. Several recent publications have also reported luminescence from these silver nanoparticles, in particular silver oxide particles, with envisaged applications in optical storage [49]. Recent microscopy studies of nanoscale silver oxide reveals strong photoactivated emission for excitation wavelengths shorter than 520 nm, with multicolor blinking, even from single nanoparticles. The individual luminescent species are thought to be silver nanostructures that are photochemically generated from the oxide [49], where the several Ag atom nanoclusters show a strongly size-dependent luminescence [50].

2.3 Silica as a Shell

Coatings of colloidal particles with silica layer have many advantages, because such a shell is chemically inert and optically transparent. Furthermore, the colloid chemistry of silica is well understood, and many possibilities for surface modification are available. Coating by silica in a seeded growth process [51-53] leads to a decrease in the polydispersity of the particles and reduces the van der Waals attraction, which enhances the colloid stability and ability to form colloidal crystals. The thin silica layer increases the mechanical stability,

makes possible a transfer into organic solvents, provides for a capping layer on the semiconductor nanocrystals, and protects metal particles against oxidation.

2.4 Core/Shell Nanoparticles

Controlled fabrication of nanomaterials has been one of the challenges faced by nanotechnologists and only limited progress has been achieved so far. One of the fascinating characteristics of nanomaterials is that their properties are dependent on size, shape, composition and structural order. Therefore, it is imperative to develop effective and reliable methodologies to cater to the ever increasing demands of tailored nanomaterials with the desired properties. Core/shell nanoparticles, i.e. particles with a well-defined core and shell, both in nanometer range, have demanding applications in pharmaceuticals, chemical engineering, biology, optics, drug delivery and many other related areas in addition to chemistry.

Coating a given ensemble of nanoparticles by another material yields core/shell nanocrystals. In these structures, the cores may be of any kind of colloidal particles, i.e. metals, insulators, and all classes of semiconductors. Likewise, the shell may consist of any sort of materials including organic ones.

In majority cases, the electronic structure of core/shell particles is as follows. The core material having a certain bandgap is capped by a material with a larger band gap, the conduction band energy of the capping material being higher (more negative in an electrochemical sense) than that of the core material and the valance band energy of the capping material being lower (more positive on the electrochemical energy scale) than that of the core material. This energetic situation is frequently called a type-1 structure. The main consequences of this capping is that the exciton photogenerated in the core is prevented from spreading over the entire particle, and by this it is forced to recombine while spatially confined to the core. In most cases this is accompanied by enhanced luminescence.

During the past decade, there have been widespread research efforts to develop core/shell colloidal nanoparticles with tailored structural, optical, surface and other properties. [54-

56]. Investigations on these types of materials have been catalyzed by their applicability in modern science and their technological edge over conventional materials. Such composite coatings are used in sensors (for protecting high-tech equipments from lasers in the form of optical limiters), nanoelectronics, catalysis and pharmaceuticals. The term used to describe synthesis of core-shell particles with well-defined morphologies and tailored properties is called 'particle engineering'. This is achieved by encapsulating the nanometal core within the shell of a preferred material, or by coating the nanoparticle core with the shell material. The shell protection imparts certain functional properties to the nanomaterial including: (1) monodispersity in size, (2) core and shell processibility, (3) solubility and stability, (4) ease of self-assembly, and (5) application in nanoscale optics, nanoelectronics, as well as in magnetic, catalytic, chemical and biological fields. Shell protection is absolutely necessary for the following important reasons: (a) the shell can alter the surface charge, reactivity and functionality of the metal core thereby enhancing the stability and dispersibility of the colloidal materials; (b) by choosing a suitable shell-forming material, we can incorporate magnetic, optical and catalytic properties into the composite material; (c) encasing the metal core in a shell invariably protects it from physical and chemical changes; and (d) core-shells exhibit improved physical and chemical characteristics as compared to their single component counterparts.

Semiconductor nanocrystals exhibit interesting size-dependent optical properties because of the confinement of electronic wavefunctions. Control of their surface is the key to highly luminescent nanocrystals. This is because of the presence of a large number of surface defects arising form nonstochiometry, unsaturated bonds, etc. core/shell type composite quantum dots exhibit novel properties which make them attractive for chemists. Overcoating the nanocrystallites with higher band gap inorganic materials have been shown to increase the photoluminescence quantum yield due to passivation of surface non-radiative recombination sites. Also, particles passivated with inorganic composite materials are much more reliable and robust than their corresponding organic analogues.

2.4.1 Applications of Core/Shell nanoparticles

Biological applications

Magnetic core/shell nanoparticles are used in clinical applications and biotechnology, as the shells can be made biocompatible. Such core/shell particles find use in hyperthermia as immunoassays. They also find extensive uses in the transportation of the drugs to the site of diseases, and function as magnetic carriers for the identification and isolation of blood cells and antibodies. Further they are used in imaging for the magnetic mapping of organs, tissue repair, detoxification of biological fluids, drug delivery and in cell separation.

Magnetism of core/shell nanoparticles

The magnetism of core/shell nanoparticles can be tuned by varying the shell thickness. The $Fe_{58}Pt_{42}$ / Fe_3O_4 core/shell nanoparticles are ferromagnetic at low temperatures, but super-paramagnetic at room temperature. Such materials find application in ultra high density magnetic storage media, biological labeling and detection and drug delivery. Core/shell type magnetic nanosystems are also of great interest from the technological point of view. Magnetic nanoparticles are used in various areas such as bearing, seals, lubricants, heat carriers, printing, recording and polishing media. One of the rapidly emerging applications of magnetic nanoparticles is in biologically labeled areas including MRI, drug delivery, rapid biological separations and therapy.

Catalysis

Catalysis by core/shell nanoparticles is a very important, active and emerging area, which can have a tremendous impact in the chemical industry, pharmaceutical products and the fuel sector. More than 90% of all industrial processes are catalytically controlled. Enhancement in specific catalytic activity and selectivity coupled with a reduction in the cost of catalysts would benefit the industrial sector in a big way. Catalysis of core/shell particles can either be due to the core or due to the shell.

The specific features which were seen to enhance the utility of the nanoparticles in the catalytic industry were their large surface-to-volume ratio and the specific binding sites on them. Nanosized gold has high catalytic activity in the oxidation and reduction of hydrocarbons. Monolayer-encapsulated Au and alloy core-shell nanoparticles are model building blocks for devising nanostructured catalysts. Tremendous variation can be achieved in the catalytic activity by changing the composition of the core, size, shape and surface properties.

Catalysis by shell includes asymmetric catalysis and mediated electrotransfer. In catalysis by nanoparticle cores, three types of nanoparticles are of relevance. These are: (a) nanoparticles supported on oxides including core/shell nanoparticles or polymers, (b) nanoparticles encapsulated in dendrimers and (c) nanoparticles encapsulated in alkane thiolate monolayers.

In order to exploit core/shell nanoparticle-based catalysis, the most important issue that must be addressed is the surface passivation of nanoparticles. This can be enhanced by place exchange, interparticle linking, size processing, electrochemical, thermal and photochemical annealing.

Sensing

The most important challenge in the field of chemical / biological sensors is the rational design of materials with high sensitivity and selectivity. Nanostructured materials provide challenging opportunities for addressing problems because of their new and unique interparticle spatial and chemical properties that can be fine-tuned with various parameters. The sensing properties are highly dependent on several design parameters such as particle size, interparticle distances and the dielectric constant of the surrounding medium.

2.5 Characterization

Materials characterization represents many different disciplines depending upon the background of the user. These concepts range from that of the scientist, who thinks of it in atomic terms, to that of the process engineer, who thinks of it in terms of properties,

procedures, and quality assurance, to that of the mechanical engineer, who thinks of it in terms of stress distributions and heat transfer. The definition selected for the ASM-International Materials Characterization Handbook is as follows: "Characterization describes those features of composition and structure (including defects) of a material that are significant for a particular preparation, study of properties, or use, and suffice for reproduction of the material." This definition limits the characterization methods included in the Handbook to those that provide information about composition, structure, and defects and excludes those methods that yield information primarily related to materials properties, such as thermal, electrical, and mechanical properties.

2.5.1 X-Ray Diffraction (XRD)

XRD is very important experimental technique that has long been used to address all issues related to the crystal structure of solids, including lattice constants and geometry, identification of unknown materials, orientation of single crystals, preferred orientation of polycrystals, defects, stresses, etc.

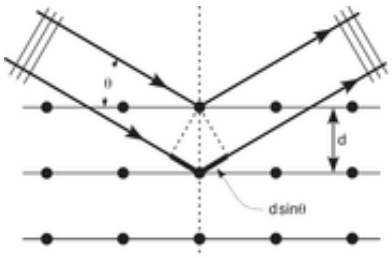

Figure 2.2: Schematic for Bragg's law

Crystals are regular arrays of atoms, and X-rays can be considered waves of electromagnetic radiation. Atoms scatter X-ray waves, primarily through the atoms' electrons. Just as an ocean wave striking a lighthouse produces secondary circular waves emanating from the lighthouse, so an X-ray striking an electron produces secondary spherical waves emanating from the electron. This phenomenon is known as scattering, and the electron (or lighthouse) is known as the scatterer. A regular array of scatterers produces

a regular array of spherical waves. Although these waves cancel one another out in most directions (destructive interference), they add constructively in a few specific directions, determined by Bragg's law

$$2d \sin \theta = n\lambda \tag{2.4}$$

where *n* is any integer. These specific directions appear as spots on the diffraction pattern, often called *reflections*. Thus, X-ray diffraction results from an electromagnetic wave (the X-ray) impinging on a regular array of scatterers (the repeating arrangement of atoms within the crystal).

X-rays are used to produce the diffraction pattern because their wavelength λ is typically the same order of magnitude (1-100 Angstroms) as the spacing *d* between planes in the crystal. To produce significant diffraction, the spacing between the scatterers and the wavelength of the impinging wave should be roughly similar in size. However, visible light has too long a wavelength (typically, 5500 Angstroms) to observe diffraction from crystals. However, prior to the first X-ray diffraction experiments, the spacings between lattice planes in a crystal were not known with certainty.

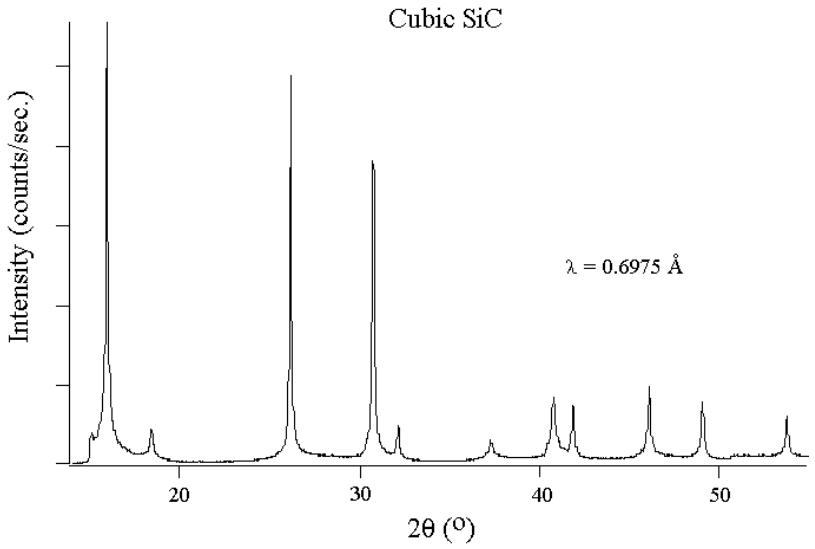

Figure 2.3: X-Ray diffraction pattern of Cubic SiC using synchrotron radiation.

2.5.1.1 Uses of XRD

Relative to other methods of analysis, powder diffraction allows for rapid, non-destructive analysis of multi-component mixtures without the need for extensive sample preparation. So, XRD can be used to analyze unknown materials and perform materials characterization in such fields as metallurgy, mineralogy, forensic science, archeology, condensed matter physics, and the biological and pharmaceutical sciences. Identification is performed by comparison of the diffraction pattern to a known standard or to a database such as the International Centre for Diffraction Data's Powder Diffraction File or the Cambridge Structural Database (CSD). The most widespread use of powder diffraction is in the identification and characterization of crystalline solids, each of which produces a distinctive diffraction pattern. Both the positions (corresponding to lattice spacings) and the relative intensity of the lines are indicative of a particular phase and material, providing a "fingerprint" for comparison. Powder XRD can be used to determine the crystallinity by comparing the integrated intensity of the background pattern to that of the sharp peaks.

The position of a diffraction peak is independent of the atomic positions within the cell and entirely determined by the size and shape of the unit cell of the crystalline phase. Each peak represents a certain lattice plane and can therefore be characterized by a Miller index.

Also, XRD can be used to determine phase transitions i.e. if the transition produces another crystalline phase, one set of lines will suddenly be replaced by another set.

2.5.2 Energy Dispersive X-Ray Spectroscopy

Energy dispersive X-ray spectroscopy (EDS, EDX or EDXRF) is an analytical technique used for the elemental analysis or chemical characterization of a sample. It is one of the variants of XRF. As a type of spectroscopy, it relies on the investigation of a sample through interactions between electromagnetic radiation and matter, analyzing X-rays emitted by the matter in response to being hit with charged particles. Its characterization capabilities are due in large part to the fundamental principle that each element has a unique atomic structure allowing X-rays that are characteristic of an element's atomic structure to be identified uniquely from each other.

To stimulate the emission of characteristic X-rays from a specimen, a high energy beam of charged particles such as electrons or protons (see PIXE), or a beam of X-rays, is focused into the sample being studied. At rest, an atom within the sample contains ground state (or unexcited) electrons in discrete energy levels or electron shells bound to the nucleus. The incident beam may excite an electron in an inner shell, ejecting it from the shell while creating an electron hole where the electron was. An electron from an outer, higher-energy shell then fills the hole, and the difference in energy between the higher-energy shell and the lower energy shell may be released in the form of an X-ray. The number and energy of the X-rays emitted from a specimen can be measured by an energy dispersive spectrometer. As the energy of the X-rays is characteristic of the difference in energy between the two shells, and of the atomic structure of the element from which they were emitted, this allows the elemental composition of the specimen to be measured.

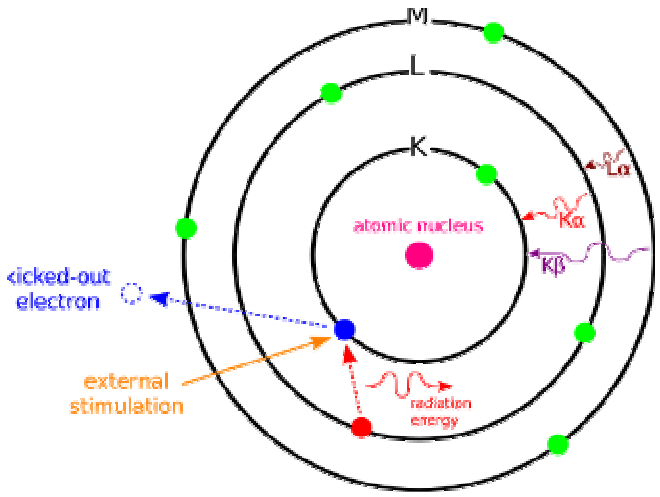

Figure 2.5: Illustration of the principle of EDX

The positions of lines (peaks with appropriate energies) give information about the qualitative composition of the sample. The number of the X-ray quanta is the measure for the concentration of the elements (peak-height). There is not linear connection between quantum numbers and concentration portions of the elements.The concentration calculation needs the net count rates or from it derived measured variables.

2.5.3 Fourier Transform Infra-Red Spectroscopy (FTIR)

Infrared (IR) spectroscopy is a chemical analytical technique, which measures the infrared intensity versus wavelength (wavenumber) of light. Based upon the wavenumber, infrared light can be categorized as far infrared (4 ~ 400cm^{-1}), mid infrared (400 ~ 4,000cm^{-1}) and near infrared (4,000 ~ 14,000cm^{-1}).

Infrared spectroscopy detects the vibration characteristics of chemical functional groups in a sample. When an infrared light interacts with the matter, chemical bonds will stretch, contract and bend. As a result, a chemical functional group tends to adsorb infrared radiation in a specific wavenumber range regardless of the structure of the rest of the molecule.

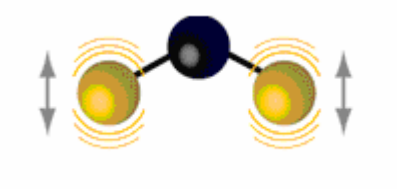

Bending mode

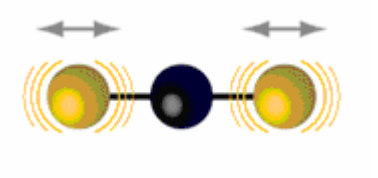

Symmetric stretching mode

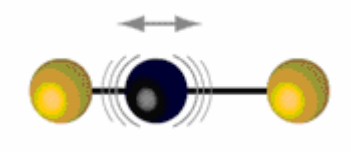

Antisymmetric stretching mode

Figure 2.6 Representation of vibrational modes

For example, the C=O stretch of a carbonyl group appears at around 1700cm^{-1} in a variety of molecules. Hence, the correlation of the band wavenumber position with the chemical structure is used to identify a functional group in a sample. The wavenember positions where functional groups adsorb are consistent, despite the effect of temperature, pressure, sampling, or change in the molecule structure in other parts of the molecules. Thus the presence of specific functional groups can be monitored by these types of infrared bands, which are called group wavenumbers.

A Fourier Transform Infrared (FTIR) spectrometer obtains infrared spectra by first collecting an interferogram of a sample signal with an interferometer, which measures all of infrared frequencies simultaneously. An FTIR spectrometer acquires and digitizes the interferogram, performs the FT function, and outputs the spectrum.

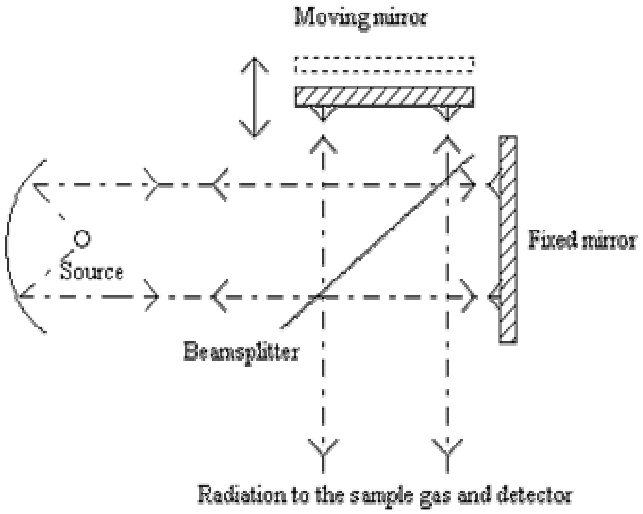

Figure 2.7: Illustrating principle of FTIR

An interferometer utilizes a beamsplitter to split the incoming infrared beam into two optical beams. One beam reflects off of a flat mirror which is fixed in place. Another beam reflects off of a flat mirror which travels a very short distance (typically a few millimeters) away from the beamsplitter. The two beams reflect off of their respective mirrors and are recombined when they meet together at the beamsplitter. The re-combined signal results from the interfering with each other. Consequently, the resulting signal is called interferogram, which has every infrared frequency "encoded" into it.

When the interferogram signal is transmitted through or reflected off of the sample surface, the specific frequencies of energy are adsorbed by the sample due to the excited vibration of function groups in molecules. The infrared signal after interaction with the sample is uniquely characteristic of the sample. The beam finally arrives at the detector and is measure by the detector. The detected interferogram can not be directly interpreted. It has to be "decoded" with a mathematical technique in term of Fourier Transformation. The computer can perform the Fourier transformation calculation and present an infrared spectrum, which plots adsorbance (or transmittance) versus wavenumber.

Figure 2.8 FTIR spectrometer

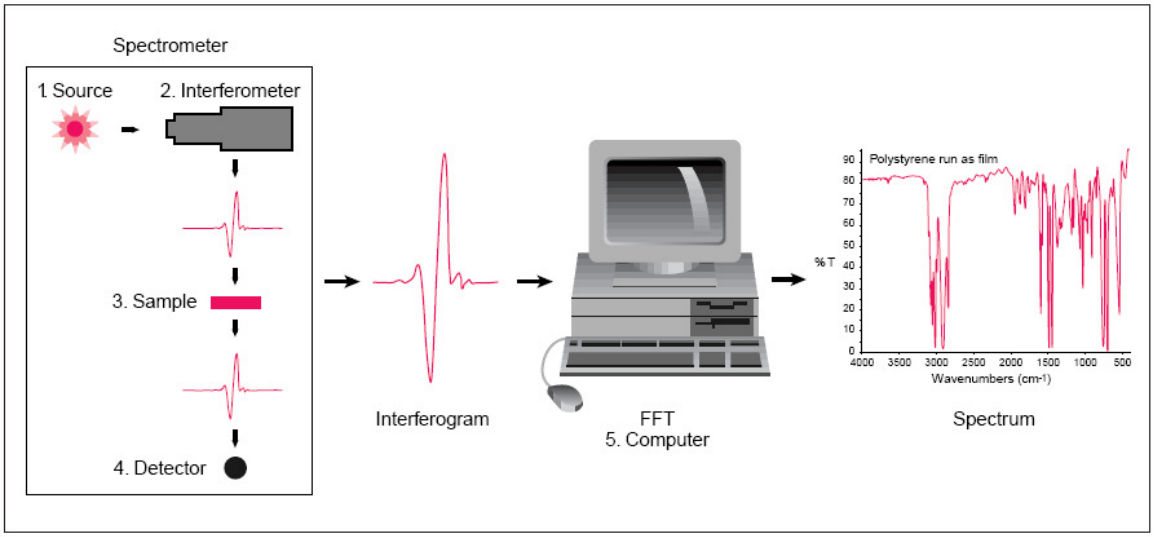

Figure 2.9 The sample analysis process.

When an interferogram is Fourier transformed, a single beam spectrum is generated. A single beam spectrum is a plot of raw detector response versus wavenumber. When an interferogram is measured with a sample and Fourier transformed, a sample single beam spectrum is obtained. It looks similar to the background spectrum except that the sample peaks are superimposed upon the instrumental and atmospheric contributions to the spectrum. To eliminate these contributions, the sample single beam spectrum must be normalized against the background spectrum. Consequently, a transmittance spectrum is obtained as follows.

$$\%T = I/Io \tag{2.5}$$

Where $\%T$ is transmittance; I is the intensity measured with a sample in the beam (from the sample single beam spectrum); Io is the intensity measured from the back ground spectrum

The absorbance spectrum can be calculated from the transmittance spectrum using the following equation.

$$A = -\log_{10} T \tag{2.6}$$

where A is the absorbance.

The final transmittance/absorbance spectrum should be devoid of all instrumental and environmental contributions, and only present the features of the sample. If the concentrations of gases such as water vapor and carbon dioxide in the instrument are the same when the background and sample spectra are obtained, their contributions to the spectrum will ratio out exactly and their bands will not occur. If the concentrations of these gases are different when the background and sample spectra are obtained, their bands will appear in the sample spectrum.

2.5.3.1 Uses of FTIR

FTIR is most useful for identifying chemicals that are either organic or inorganic. It can be utilized to quantitate some components of an unknown mixture. It can be applied to the analysis of solids, liquids, and gasses. FTIR is perhaps the most powerful tool for identifying types of chemical bonds (functional groups). The wavelength of light absorbed is characteristic of the chemical bond as can be seen in this annotated spectrum. By interpreting the infrared absorption spectrum, the chemical bonds in a molecule can be determined. FTIR spectra of pure compounds are generally so unique that they are like a molecular "fingerprint". While organic compounds have very rich, detailed spectra, inorganic compounds are usually much simpler.

Because the strength of the absorption is proportional to the concentration, FTIR can be used for some quantitative analyses. Usually these are rather simple types of tests in the concentration range of a few ppm up to the percent level. For example, the amount of silica trapped on an industrial hygiene filter is determined by FTIR using NIOSH method 7602.

2.5.4 UV- Visible spectroscopy

Ultraviolet and visible spectroscopy (UV-Vis) is a reliable and accurate analytical laboratory assessment procedure that allows for the analysis of a substance. Specifically, ultraviolet and visible spectroscopy measures the absorption, transmission and emission of ultraviolet and visible light wavelengths by matter.

When sample molecules are exposed to light having an energy that matches a possible electronic transition within the molecule, some of the light energy will be absorbed as the electron is promoted to a higher energy orbital. An optical spectrometer records the wavelengths at which absorption occurs, together with the degree of absorption at each wavelength. The resulting spectrum is presented as a graph of absorbance (A) versus wavelength.

A beam of light from a visible and/or UV light source (colored red) is separated into its component wavelengths by a prism or diffraction grating. Each monochromatic (single

wavelength) beam in turn is split into two equal intensity beams by a half-mirrored device. One beam, the sample beam (colored magenta), passes through a small transparent container (cuvette) containing a solution of the compound being studied in a transparent solvent. The other beam, the reference (colored blue), passes through an identical cuvette containing only the solvent. The intensities of these light beams are then measured by electronic detectors and compared. The intensity of the reference beam, which should have suffered little or no light absorption, is defined as $\mathbf{I_0}$. The intensity of the sample beam is defined as **I**. Over a short period of time, the spectrometer automatically scans all the component wavelengths in the manner described. The ultraviolet (UV) region scanned is normally from 200 to 400 nm, and the visible portion is from 400 to 800 nm.

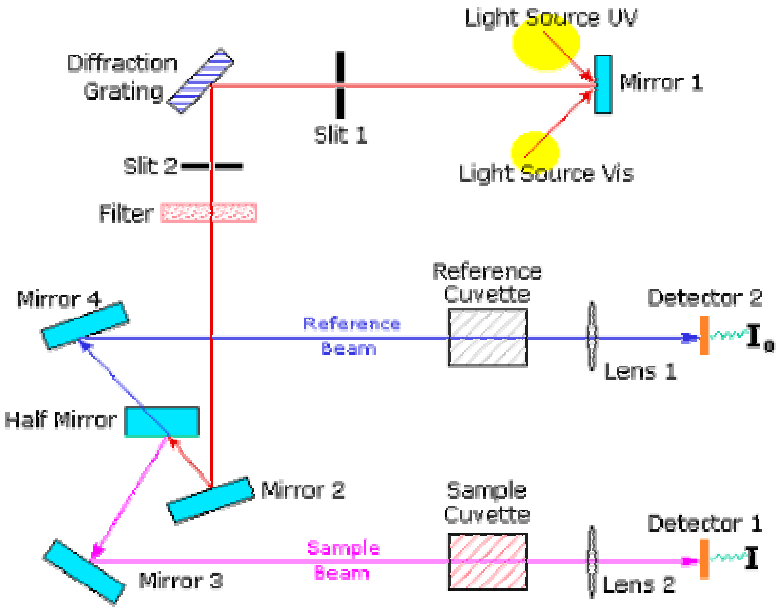

Figure 2.10 Illustrating the principle of UV-Visible spectroscopy

UV/vis spectrophotometer measures the intensity of light passing through a sample (I), and compares it to the intensity of light before it passes through the sample (I_o). The ratio I / I_o is called the transmittance, and is usually expressed as a percentage (%T). The absorbance, A, is based on the transmittance:

$$A = -\log (\%T / 100\%) \quad (2.7)$$

In the practical sense, spectroscopy measures the absorption, emission, or scattering of electromagnetic radiation by atoms or molecules. By such measurements, the type of the atoms or molecules present in a sample, as well as a measure of their concentration or abundance can be made. Absorption of ultraviolet or visible light electromagnetic radiation causes electron to move from lower energy levels to a higher energy levels. Ultraviolet-visible absorption spectroscopy measures the absorption of ultraviolet or visible light. Because the spectrum of an atom or molecule depends on its electron energy levels, UV-visible absorption spectra are useful for identifying unknown substances.

2.5.5 Photoluminescence (PL)

Luminescence refers to the emission of light by a material through any process other than black body radiation. The emission of light can result from variety of stimulations. For example, when the emission is resulted from electronic stimulation, it is referred to as cathodoluminescence (CL). When X-rays are used to excite the sample it is called X-ray fluorescence. In photoluminescence photons are incident on the material. So when light of sufficient energy is incident on a material, photons are absorbed and electronic excitations are created. Eventually, these excitations relax and the electrons return to the ground state. If radiative relaxation occurs, the emitted light is called PL. This light can be collected and analyzed to yield a wealth of information about the photoexcited material. The PL spectrum provides the transition energies, which can be used to determine electronic energy levels. The PL intensity gives a measure of the relative rates of radiative and non-radiative recombination. Variation of the PL intensity with external parameters like temperature and applied voltage can be used to characterize further the underlying electronic states and bands.

Typically light is directed onto the sample for excitation and the emitted luminescence is collected by a lens and passed through an optical spectrometer onto a photon detector. The spectral distribution and time dependence of the emission are related to the electronic transition probabilities within the sample, and can be used to provide qualitative and

sometimes quantitative information about the chemical composition, structure, impurities, kinetic process and energy transfer.

Because PL often originates near the surface of a material, PL analysis is an important tool in the characterization of surfaces. The utility of PL for this purpose is derived from its unique sensitivity to discrete electronic states, many of which lie near surfaces and interfaces. Using the techniques noted above, the nature of these states can be probed in detail. The energy distribution and density of interface states can be ascertained by studying the excitation intensity dependence of the PL spectrum.

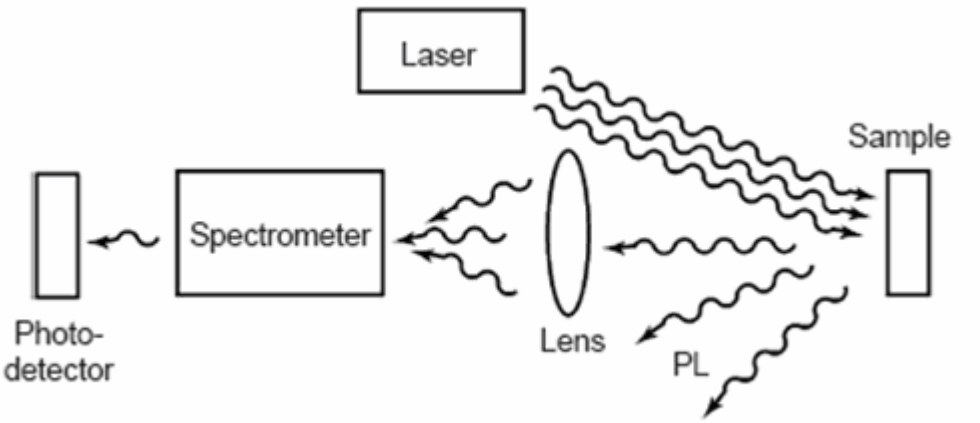

Figure 2.11: Experimental set-up for PL measurements

2.5.5.1 Forms of photoluminescence

The simplest photoluminescent processes are **resonant radiations**, in which a photon of a particular wavelength is absorbed and an equivalent photon is immediately emitted. This process involves no significant internal energy transitions of the chemical substrate between absorption and emission and is extremely fast, of the order of 10 nanoseconds.

In fluorescence, the chemical substrate undergoes internal energy transitions before re-emitting the energy from the absorption event. This is also typically a fast process, but in which some of the original energy is dissipated so that the emitted light photons are of lower energy than those absorbed.

In phosphorescence, the energy from absorbed photons undergoes intersystem crossing into a state of higher spin multiplicity, usually a triplet state. Once the energy is trapped in the triplet state, transition back to the lower singlet energy states is quantum mechanically forbidden, meaning that it happens much more slowly than other transitions. The result is a slow process of radiative transition back to the singlet state, sometimes lasting minutes or hours.

2.5.5.2 Uses of Photoluminescence

The most common radiative transition in semiconductors is between states in the conduction and valence bands, with the energy difference being known as the band gap. Band gap determination is particularly useful when working with new compound semiconductors.

Radiative transitions in semiconductors also involve localized defect levels. The photoluminescence energy associated with these levels can be used to identify specific defects, and the amount of photoluminescence can be used to determine their concentration.

The return to equilibrium, also known as recombination, can involve both radiative and non- radiative processes. The amount of photoluminescence and its dependence on the level of photo-excitation and temperature are directly related to the dominant recombination process. Analysis of photoluminescence helps to understand the underlying physics of the recombination mechanism.

In general, non-radiative processes are associated with localized defect levels, whose presence is detrimental to material quality and subsequent device performance. Thus, material quality can be measured by quantifying the amount of radiative recombination.

2.5.5.3 Special Features of Photoluminescence spectroscopy

- Various excitation wavelengths allow for varying penetration depths into the material, and thus, varying levels of volume excitation.
- Detection of photoluminescence from 0.4 to 2.8 micrometers using diffraction and Fourier-transform-based systems.

- Mapping capabilities with 1-micrometer spatial resolution on the Fourier-transform-based system.
- Sample temperatures of 4 to 300 K.
- Sensitivity down to the level of parts per thousand, depending on impurity species and host.

CHAPTER 3

EXPERIMENTAL DETAILS

3.1 Core/shell nanocrystals

The emission color from semiconductor nanocrystal quantum dots is tunable by the size as a result of the quantum-confinement effect [57, 58]. Harnessing this emission for real-world applications such as biological fluorescence marking [59, 60] and optoelectronic devices [61-65] is an important challenge, which imposes stringent requirements for a high florescence quantum yield (QY) and stability against photo-degradation. These characteristics are difficult to achieve in semiconductor nanocrystals coated with organic ligands because of imperfect surface passivation. In addition, the organic ligands are labile in exchange reactions because of their weak bonding to the nanocrystal surface atoms [66]. A proven strategy for increasing both the fluorescence QY and the stability is to grow a shell of a higher band gap semiconductor on the core nanocrystal [61-72]. In such composite core/shell structures, the shell type and the shell thickness provide further control for tailoring the optical, electronic, electrical and chemical properties of semiconductor nanocrystals.

The core/shell approach is conceptually closely related to the approach used in two-dimensional quantum wells [73]. In a quantum well, a thin layer, of nanometric dimensions, of a low band gap semiconductor is sandwiched between thick layers of a high band gap semiconductor, forming a square potential well for the electron and hole wavefunctions. The determining factor for the growth of quantum wells is the lattice mismatch between the two semiconductors. The electronic properties of the quantum well are determined primarily by the energetic offsets between the conduction and valance band edges of the two semiconductors.

3.2 The Sol-Gel Technique

The sol-gel technique is based on hydrolysis of liquid precursors and formation of colloidal sols. The precursors are usually organosilicates (e.g. TEOS - tetraethoxysilane) yielding silicate sol-gel materials. However, the method is not restricted to the silicon compounds - for example compounds of zirconium, vanadium etc. can be used as precursors leading to materials possessing different physico-chemical properties. Furthermore, it is possible to

obtain modified organosilicates precursors with direct Si-C bonds (which do not undergo hydrolysis) and possessing terminal functional groups (e.g. -NH2, -SH2 etc.). Such precursors, either pure or mixed with the conventional ones, yield inorganic-organic materials with mechanical (e.g. elasticity) and physico-chemical properties (e.g. wetability) modified by the organic components of the inorganic polymer network. The functional groups can be also used for covalent binding of various chemicals (including biomolecules) giving specifically modified glassy materials.

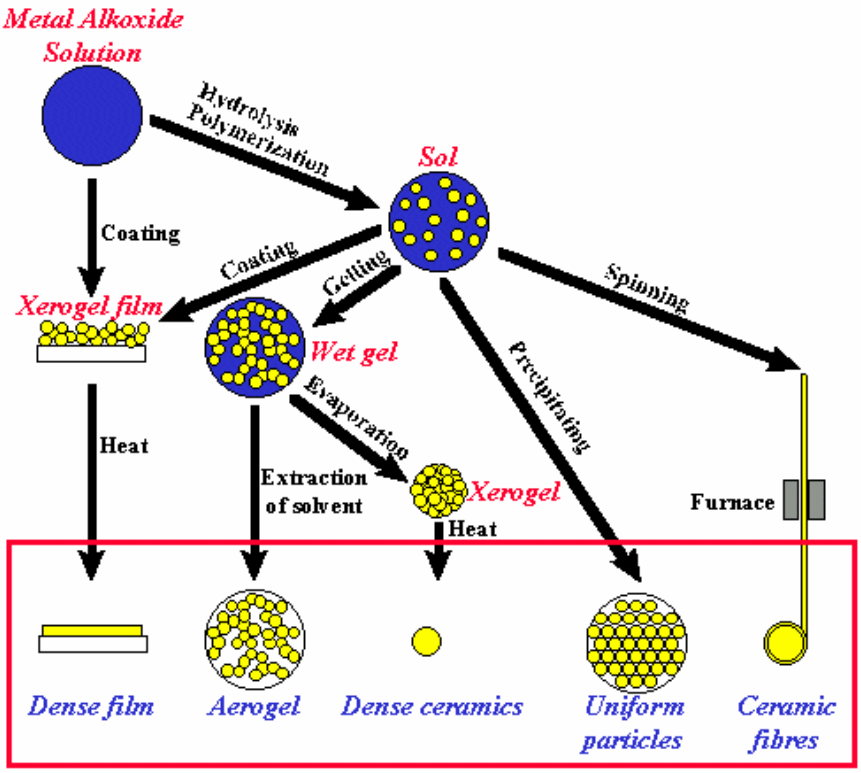

Figure 3.1: Schematic representation of the sol-gel process

The sol-gel process is a wet-chemical technique for the fabrication of materials (typically a metal oxide) starting either from a chemical solution (*sol* short for solution) or colloidal particles (*sol* for nanoscale particle) to produce an integrated network (*gel*). Typical

precursors are metal alkoxides and metal chlorides, which undergo hydrolysis and polycondensation reactions to form a colloid, a system composed of solid particles (size ranging from 1 nm to 1 μm) dispersed in a solvent. The sol evolves then towards the formation of an inorganic continuous network containing a liquid phase (*gel*). Formation of a metal oxide involves connecting the metal centers with oxo (M-O-M) or hydroxo (M-OH-M) bridges, therefore generating metal-oxo or metal-hydroxo polymers in solution. The drying process serves to remove the liquid phase from the gel thus forming a porous material, then a thermal treatment (*firing*) may be performed in order to favor further polycondensation and enhance mechanical properties.

The precursor sol can be either deposited on a substrate to form a film (e.g. by dip-coating or spin-coating), cast into a suitable container with the desired shape (e.g. to obtain a monolithic ceramics, glasses, fibers, membranes, aerogels), or used to synthesize powders (e.g. microspheres, nanospheres). The sol-gel approach is interesting in that it is a cheap and low-temperature technique that allows for the fine control on the product's chemical composition, as even small quantities of dopants, such as organic dyes and rare earth metals, can be introduced in the sol and end up in the final product finely dispersed. It can be used in ceramics manufacturing processes, as an investment casting material, or as a means of producing very thin films of metal oxides for various purposes. Sol-gel derived materials have diverse applications in optics, electronics, energy, space, (bio) sensors, medicine (e.g. controlled drug release) and separation (e.g. chromatography) technology.

The interest in sol-gel processing can be traced back in the mid-1880s with the observation that the hydrolysis of tetraethyl orthosilicate (TEOS) under acidic conditions led to the formation of SiO_2 in the form of fibers and monoliths [74]. Sol-gel research grew to be so important that in the 1990s more than 35,000 papers were published worldwide on the process.

3.2.1 Applications of Sol-Gel Technique

Sol-gel method has been used to produce the world's lightest materials and some of its toughest ceramics.

The applications for sol gel-derived products are numerous. One of the largest application areas is thin films, which can be produced on a piece of substrate by spin-coating or dip-coating. Other methods include spraying, electrophoresis, inkjet printing or roll coating. Optical coatings, protective and decorative coatings, and electro-optic components can be applied to glass, metal and other types of substrates with these methods.

Cast into a mold, and with further drying and heat-treatment, dense ceramic or glass articles with novel properties can be formed that cannot be created by any other method. Macroscopic optical elements and active optical components as well as large area hot mirrors, cold mirrors, lenses and beam splitters all with optimal geometry can be made quickly and at low cost via the sol-gel route.

With the viscosity of a sol adjusted into a proper range, both optical and refractory ceramic fibers can be drawn which are used for fiber optic sensors and thermal insulation, respectively.

Ultra-fine and uniform ceramic powders can be formed by precipitation. These powders of single- and multicomponent compositions can be made in submicrometre particle size for dental and biomedical applications. Composite powders have been patented for use as agrochemicals and herbicides. Also powder abrasives, used in a variety of finishing operations, are made using a sol-gel type process.

One of the more important applications of sol-gel processing is to carry out zeolite synthesis. Other elements (metals, metal oxides) can be easily incorporated into the final product and the silicalite sol formed by this method is very stable.

Other products fabricated with this process include various ceramic membranes for microfiltration, ultrafiltration, nanofiltration, pervaporation and reverse osmosis.

If the liquid in a wet gel is removed under a supercritical condition, a highly porous and extremely low density material called aerogel is obtained. Drying the gel by means of low temperature treatments (25-100 ^{0}C), it is possible to obtain porous solid matrices called xerogels.

Finally of historical note, a sol-gel process was developed in the 1950s for the production of radioactive powders of UO_2 and ThO_2 for nuclear fuels, without generation of large quantities of dust.

3.3 Synthetic Strategy

The first step in the synthesis of a nanocrystal is the nucleation of the particles. Successful nucleation is an indication of whether the reaction in question is appropriate for the formation of nanocrystals. For a monodisperse sample, the nucleation event must be well separated in time from the growth step, which generally means that nucleation must occur on a short time scale, of the order of a fraction of a second. In contrast, if nucleation is spread out in time such that nucleation and growth overlap, different nucleation sites will undergo growth of different durations, resulting in a broad size distribution.

An effective way to achieve separation of nucleation from growth is the use of a method of injecting suitable precursors at high temperature such that nucleation occurs immediately on contact with the hot solvent. This method has been perfected in the preparation of CdSe nanocrystals [75, 76].

The next stage in the nanocrystal synthesis is the growth of the particles. As with nucleation, intermediate species and the growing particle must stay in solution throughout the process. Growth is completed when the reagents are consumed, although additional high-temperature annealing time may be needed to obtain good crystallinity. Under prolonged high-temperature annealing the possibility of Ostwald ripening arises- an undesired mechanism that will broaden the size distribution [78]. Growth can also be effectively quenched by cooling the reaction mixture. A typical behavior during the growth stage was found by Alivisatos and coworkers, who studied the growth if both CdSe and InAs nanocrystals and introduced the important concept of size focusing [76]. This concept is based on the existence of a critical size that depends on the reaction conditions such as concentration of reactants, temperature, solvent etc. Above the critical size, growth rate decreases with increased size, leading to a narrowing or focusing of the size distribution, while below the critical size, defocusing results because the growth rate of smaller particles is slower than that of the bigger particles. To achieve a narrow distribution, conditions

should be optimized so that during growth the reaction remains within the size focusing conditions.

An additional critical issue for high quality nanocrystals is the passivation of the surface. During the synthesis, surface passivation helps to control the growth of the nanocrystal, prevents agglomeration and focusing of particles, and provides for the solubility of the nanocrystals in common solvents. Solvation is important not only for nanocrystals, but also for the reactants and intermediates. Surface passivation is achieved by using an organic molecule to coordinate or bond to the reaction. This strategy benefits from having the capping molecule in huge excess and from having a common solvation medium for the reactants, intermediates, and nanocrystals.

Capping groups typically contain an electron-rich donating group such as phosphine oxides, phosphines, amines, or thiols and behave as Lewis base, which co-ordinates to the electron-poor Lewis acid-like metal of the semiconductor such as cadmium or indium. This coordination passivates the dangling orbitals at the nanocrystal surface, preventing further growth or agglomeration. The other end of the ligand imparts solubility to the nanocrystal by giving the particle a hydrophilic or hydrophobic surface.

Surface passivation plays an important role not only during the synthesis. It can also be used to further derivatize the surface of the particles, providing additional chemical control to attach nanocrystals to a surface [79], to electrodes [80], to other nanocrystals, and to biomolecules [81]. Because of the relatively weak coordination bonds of most-capping groups, these molecules can easily be exchanged after the initial synthesis. Many of the properties of the nanocrystals, notably photoluminescence, are sensitive to the surface passivation, and the manipulation of the surface-capping groups can be used to tune these properties [82, 83].

Chemicals Used

Cadmium nitrate ($Cd(NO_3)_2.4H_2O$)	Mol. Weight: 308.48 g
Sodium sulfide flakes (Na_2S)	Mol. Weight: 78.05 g

Tetraethyl orthosilicate (TEOS) ($C_8H_{20}O_4Si$) Mol. Weight: 208.33 g

Ethanol (CH_3CH_2OH) Mol. Weight: 46.08

Experimental details

The CdS/SiO_2 core-shells were synthesized using sol-gel technique.

1) 0.1 M cadmium nitrate (3.08 g) in 100 ml of water and 0.2 M sodium sulfide (1.5 g) in 100 ml of water was mixed together. Say it solution I.
2) 5 ml of tetra ethyl orthosilicate (TEOS), 10 ml ethanol, and 10 ml distilled water were mixed together and the pH was set to approximately 2.0 by adding dilute H_2SO_4. Marked it solution II.
3) X ml of 0.1 N $AgNO_3$ solution is mixed with 0.63 g of oxalic acid in 50 ml of water. Where X = 5,10,15,20 ml. let it be solution III.

For undoped CdS/SiO_2 core-shells solution I and II were mixed together. Then refluxing was done at 80 ^oC for 3 hours. **The sample was named as Ag0.** For the synthesis of CdS/SiO_2 core-shells doped with silver first solution I and II are mixed together and then III solution is added. Then refluxing was done at 80 ^oC for 3 hours. **The samples were named as Ag1 for X=5 ml, Ag2 for X=10 ml, Ag3 for X=15 ml and Ag4 for X=20 ml.**

The refluxed solution was then precipitated using Whatmann`s filter paper. Then the precipitates were washed several times with double distilled water and ethanol, and were dried in an open air oven at 80 ^oC for around a day. The dried samples were slightly crushed and preserved in air tight containers for the further characterizations.

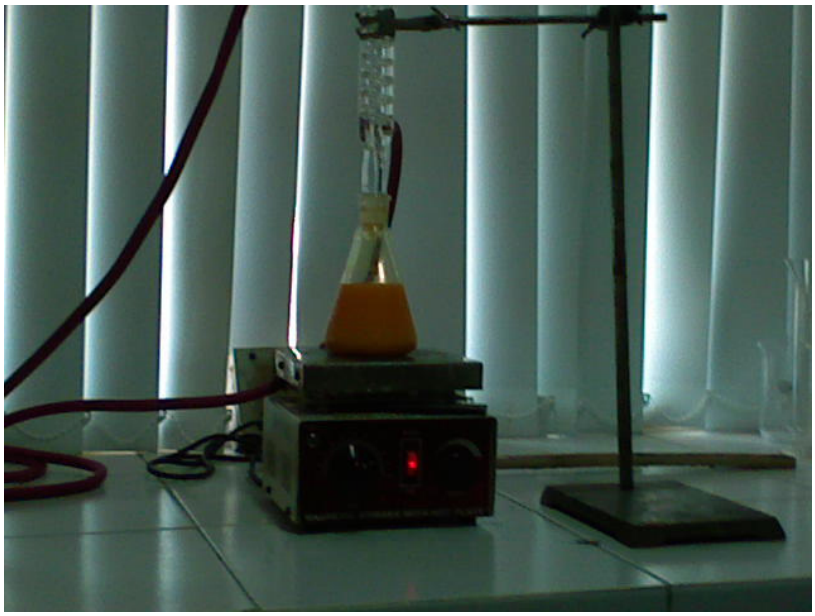

Figure 3.2: Pictorial view of the reflux at 80 ^{o}C, during the sol-gel synthesis

Figure 3.3: Pictorial view of the precipitation process, during the synthesis of Ag doped CdS/Silica nanoparticles

CHAPTER 4

RESULTS AND DISCUSSION

4.1 X-ray diffraction (XRD) Studies

XRD is a very important experimental technique that has long been used to address all issues related to the crystal structure of solids, including lattice constants and geometry, identification of unknown materials etc. Figure 4.1 shows the powder X-ray diffraction pattern of undoped CdS/SiO_2 core/shell nanostructures (Ag0). The diffraction peaks positioned at 2θ values of 25.208 ^{o}, 26.542 ^{o}, 27.861 ^{o}, 43.94 ^{o}, 47.629 ^{o}, 51.898 ^{o}, 70.88 ^{o} match well with hexagonal wurtzite phase of CdS (JCPDS Powder Diffraction File no. 41-1049), and can be indexed respectively to the *(100), (002), (101), (110), (103), (112)* and *(211)* crystal planes. However, as seen in figures 4.2 and 4.3, after doping CdS/SiO_2 core/shell nanoparticles with silver, it has been found that the peaks have become distinct and sharp. This shows the enhancement in the crystallinity of the CdS/SiO_2 nanoparticles on doping with Ag.

Moreover, as seen from figures 4.2 and 4.3, there are several small diffraction peaks centered between the strong peaks of CdS. These diffraction peaks centered at 2θ values of 30.430 ^{o}, 32.272 ^{o}, 33.55 ^{o}, 36.491 ^{o}, 37.847 ^{o}, 46.224 ^{0}, 47.45 ^{o}, 51.107 ^{o}, 52.894 ^{o}, 54.522 ^{o}, 61.138 ^{o}, 66.393 ^{o} and 75.624 ^{o} match well with silver oxalate (JCPDS Powder Diffraction File no. 22-1335) and correspond to (-111), (111), (-211), (-301), (211), (-411), (-321), (321), (411), (-231), (-141) and (341) crystal planes. The formation of silver oxalate is due to the following reactions:

$$\begin{array}{l} COOH \rightarrow COO^{2-} + 2H^+ \\ | \\ COOH \end{array} \qquad (4.1)$$

$$AgNO_3 \rightarrow Ag^+ + NO_3^- \qquad (4.2)$$

$$\begin{array}{l} COOH + AgNO_3 \rightarrow \\ | \\ COOH \end{array} \quad \begin{array}{l} COOAg + HNO_3 \\ | \\ COOAg \end{array} \qquad (4.3)$$

Tables 4.1, 4.2 and 4.3 show the comparison between the observed and the standard intensities of the diffraction peaks of the undoped and doped CdS/silica nanoparticles. The observed intensity of the diffraction peak corresponding to the (002) plane is much higher than that of the (101) plane. However, it was expected vice a versa according to the standard results.

.

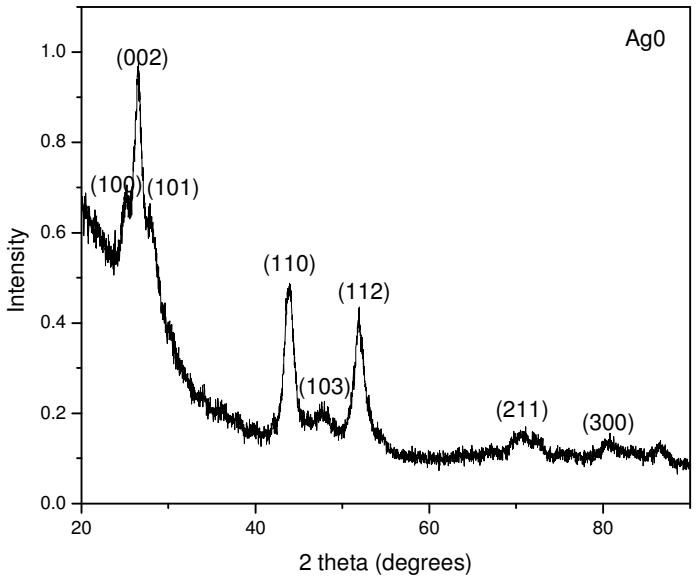

Figure 4.1: X-ray diffraction pattern of CdS/SiO_2 core/shell nanoparticles (Ag0)

2θ (degrees)	**(hkl)**	**Observed Intensity**	**Standard Intensity**
25.208	(100)	69.9	62
26.542	(002)	97.3	91
27.861	(101)	66.1	100
43.940	(110)	48.5	48
47.629	(103)	22.35	50

51.898	(112)	43.12	31
70.880	(211)	15.90	8

Table 4.1: Observed and standard data of the diffraction peaks for Ag0 sample.

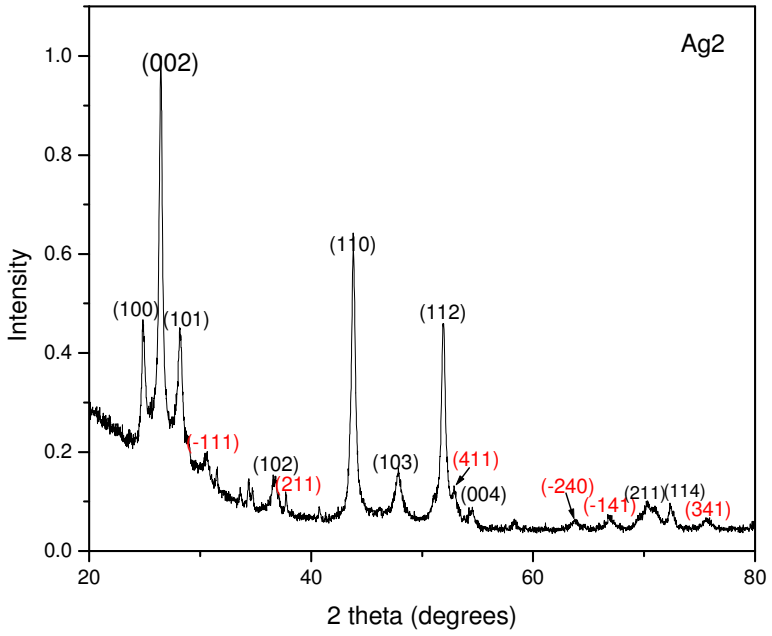

Figure 4.2: X-ray diffraction pattern of CdS/SiO_2 core/shell nanoparticles doped with silver (Ag2)

2θ (degrees)	**(hkl)**	**Observed Intensity**	**Standard Intensity**
24.840	(100)	46.79	62
26.449	(002)	98.50	91
28.163	(101)	45.07	100
36.661	(102)	15.13	29
43.883	(110)	64.17	48
47.833	(103)	15.90	50
51.921	(112)	45.61	31
52.899	(201)	13.00	15
54.459	(004)	8.90	5
58.318	(202)	6.20	3
66.850	(203)	7.57	15

70.122	(211)	10.25	8
72.430	(114)	9.7	4

Table 4.2: Observed and standard data of the diffraction peaks for Ag2 sample.

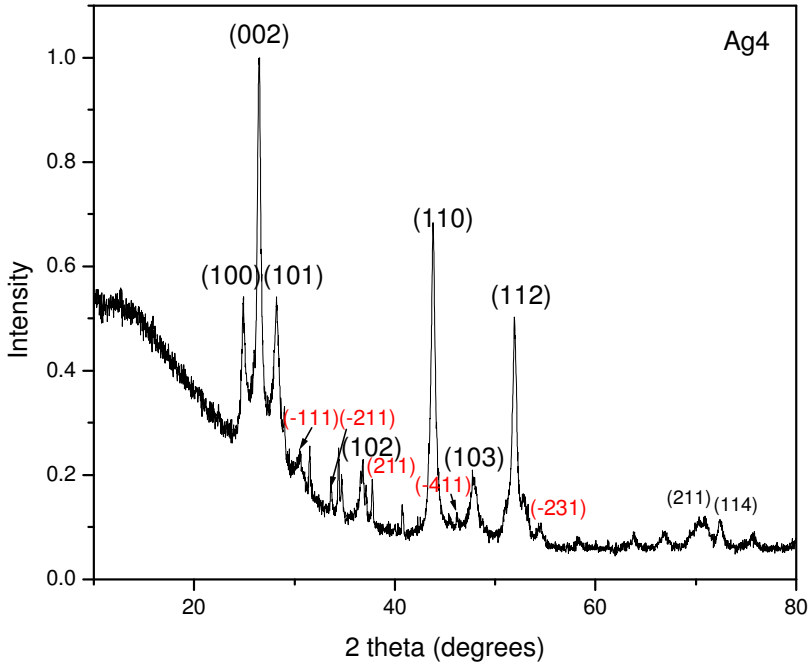

Figure 4.3: X-ray diffraction pattern of CdS/SiO_2 core/shell nanoparticles doped with silver (Ag4).

2θ (degrees)	Planes (hkl)	Observed Intensity	Standard Intensity
24.908	(100)	54.5	62
26.450	(002)	100.0	91
28.213	(101)	53.4	100
36.830	(102)	22.8	29
43.793	(110)	68.5	48
47.800	(103)	20.1	50
51.890	(112)	49.6	31
70.410	(211)	12.3	8
72.440	(114)	11.5	4

Table 4.3: Observed and standard data of the diffraction peaks for the Ag4 sample

The crystallite size, D, of the nanoparticles was found from the peak width with the Scherrer's formula:

$$\mathbf{D= 0.94\lambda/B \cos \theta} \qquad (4.1)$$

where D is the average crystallite size, λ is the X-ray wavelength, B is the full width of height maximum (FWHM) of a diffraction peak, θ is the diffraction angle.

Crystallite sizes of the three samples Ag0, Ag2, and Ag4 as calculated by Scherrer's formula is given in table 4.4. This shows that crystallite size has increased on doping the nanoparticles with silver

Sample name	Crystallite size (nm)
Ag0	23.65
Ag2	52.46
Ag4	44.70

Table 4.4: Calculated crystallite sizes of undoped and Ag doped CdS/SiO_2 nanoparticles

4.2 Energy Dispersive X-ray (EDX) Spectroscopy

The composition of the CdS/SiO_2 core/shell nanoparticles was analyzed by EDAX spectroscopy, using Noran System Six, as shown in figure 4.4. Electron beam induced inner-shell ionization and subsequent emission of characteristic fluorescence are analyzed in order to obtain the composition.

As shown in figure 4.4, Cd L-fluorescence (Lα in 3.0 to 3.5 keV energy range), S K-fluorescence (Kα in the 2-3 keV energy range) and Ag L & M-fluorescence (Lα in the energy range 3-4 keV, and Mα in the energy range 0.2 to 0.5 keV) have been observed in the Ag3 sample. This fluorescence spectrum shows the presence of Cd, S and Ag as the elementary components. Cd, S and Ag are present in the atomic percentages of 46.41,

50.37 and 3.22 %, respectively. This shows that Ag atoms have successfully replaced their Cd counterparts as dopant.

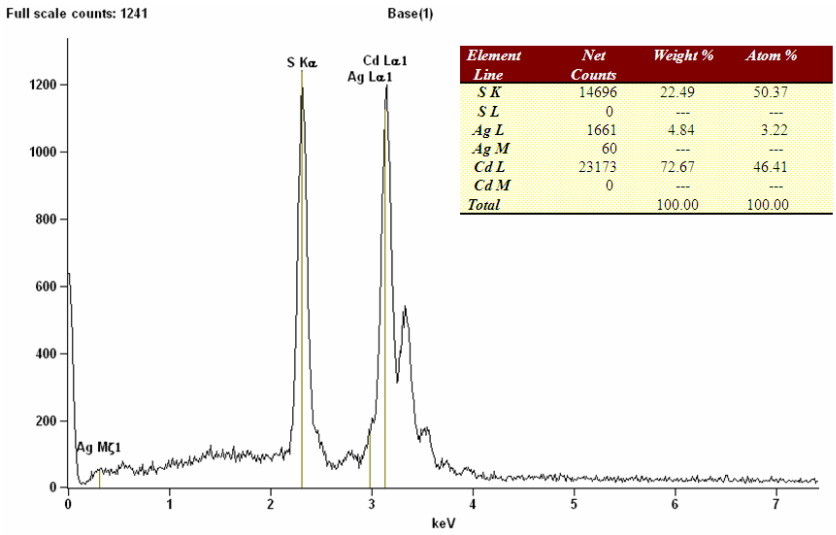

Figure 4.4: EDAX spectrum of the Ag3 sample

4.3 Fourier Transform Infrared (FTIR) Spectroscopy

The formation of CdS/SiO_2 core/shell nanoparticles was examined by recording their FTIR spectra in the range 4000 to 500 cm^{-1}. Powdered samples were used in FTIR Spectrum BX-II (Perkin Elmer) spectrometer, without any further specimen preparation.

Figure 4.5 shows the FTIR spectra of undoped and doped CdS/SiO_2 core/shell nanoparticles. Characteristic bands around 3500 cm^{-1} and 1634 cm^{-1} are ascribed to atmospheric water vapor/ethanol, which has been used during washings in the synthesis process. Moreover, the OH stretching vibrations of the SiOH group absorb in the same region. This broad band gets sharper with increasing the concentration of silver, whereas the peak at 1634 cm^{-1} has not appeared in the Ag doped samples. In CdS/SiO_2 core/shell nanoparticles, the peaks at 1058 and 801 cm^{-1} are due to the asymmetric stretching and symmetric stretching of Si-O-Si [83]. The 801 cm^{-1} weak band is due to symmetric stretching of the O atom along a line bisecting

the Si–O–Si angle, whereas the 1634 cm^{-1} peak is associated with the back and forth motion of the oxygen atom along a line parallel to the Si–Si axis. This motion results in the opposite distortion of two neighboring Si–O bonds [82].This result clearly indicates the SiO_2 layer formation on the surface of CdS nanoparticles. The sharpness of these peaks has reduced on doping with Ag. Also, weak peak centered around 3789 cm^{-1} has appeared on doping the nanoparticles with silver. The sharpness of this peak has been found to increase on increase in the concentration of Ag. These may be attributed to the N-H streching vibrations, which are the by-products of the synthesis reaction, inherited from silver nitrate solution.

The weak peaks observed at 1214 cm^{-1} can be attributed to the presence of C(=O)-O stretching vibrations in acetates or can also be due to C-H bending vibration. The FTIR peak at 801 cm^{-1} might be due to the Si-H bending. When doped with silver, Si-H bending is not observed. The bands at 2350 cm^{-1} and 667 cm^{-1} are attributed to carbon dioxide.

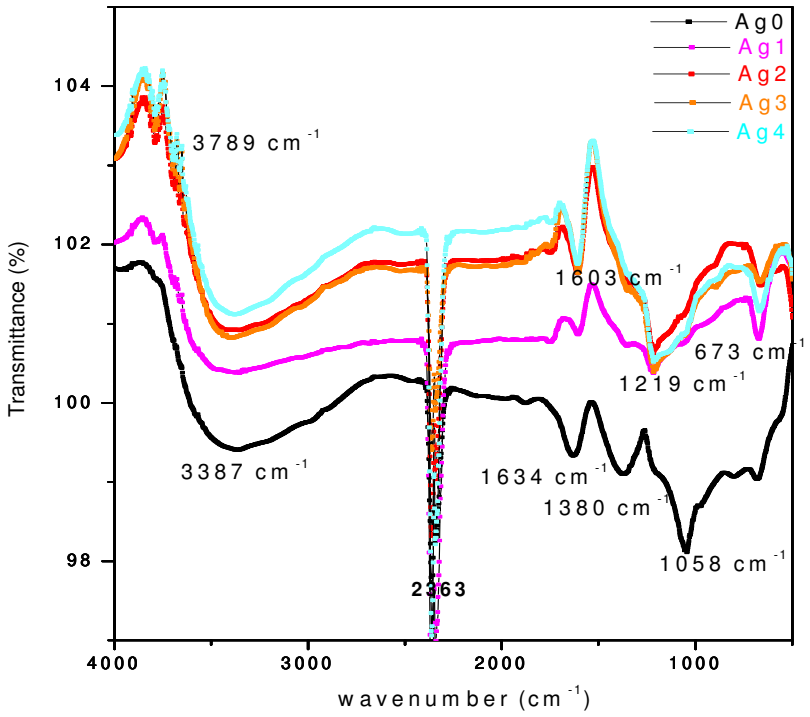

Figure 4.5: FTIR spectra of undoped and Ag doped CdS/SiO_2 nanoparticles

4.4 UV-Visible Absorption Studies

Figure 4.6 shows the UV-Visible absorption spectra of CdS/SiO_2 core/shell nanoparticles undoped and doped with different concentrations of Ag. The absorption spectra of the samples are very strong and show long absorption tails due to light scattering at high concentration of core/shell nanoparticles. The absorption onset wavelengths of samples at different doping concentrations of silver namely Ag0, Ag1, Ag2, Ag3, Ag4 are 480, 504, 509, 492 and 499 nm respectively, which are all blue-shifted compared with the absorption of bulk CdS which is 515 nm. This is because of quantum confinement effect. Also, a slight red-shift has been observed in the absorption edge on doping the nanoparticles with Ag. But no appreciable broadening or shift in the absorption band suggests that the interaction of the silver metal atoms with the CdS is week, and no surface plasmonic effects emerged on silver doping. Higher concentrations of the Ag should be tried to study the effects more prominently.

The band gap of the nanoparticles has been calculated from the differential minima of the absorbance curve. The band gap values of the CdS/SiO_2 nanoparticles are less than that of the bulk value of 2.42 eV as seen from table 4.5.

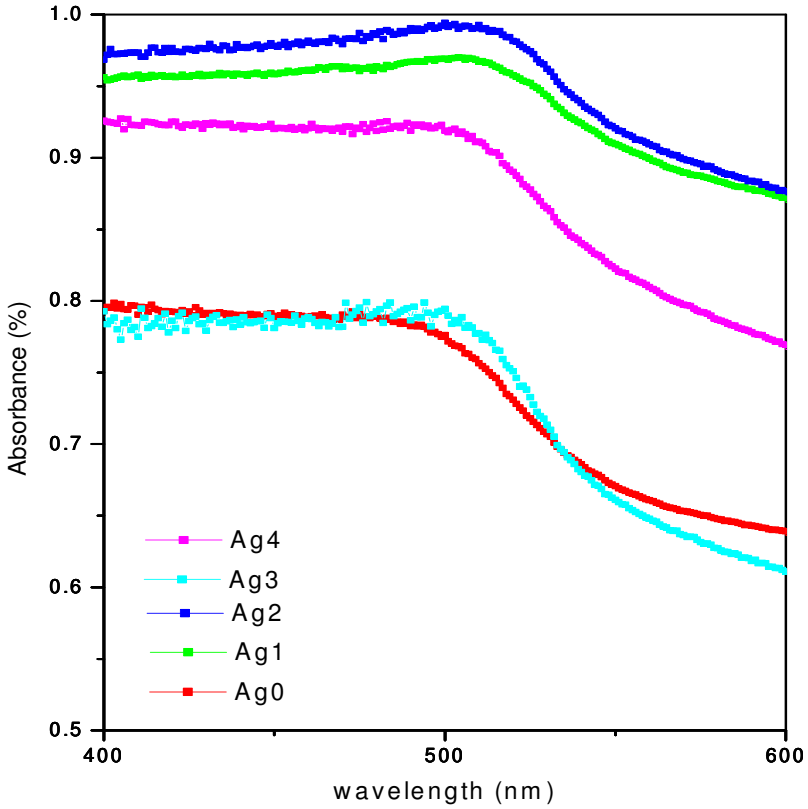

Figure 4.6: Absorption spectra of CdS/SiO_2 core/shell nanoparticles undoped and doped with silver

Sample name	Wavelength (nm)	Band gap (eV)
Ag0	517.03	2.39
Ag1	532.01	2.33
Ag2	532.01	2.33
Ag3	532.01	2.33
Ag4	532.01	2.33

Table 4.5: Calculated band gap values of the synthesized CdS/SiO_2 nanoparticles

4.5 Photoluminescence studies (PL)

Figure 4.7 shows the room temperature PL spectra of the undoped and silver doped CdS/SiO_2 nanoparticles, excited using a xenon lamp equipped within the Cary Varian`s spectrophotometer at an excitation wavelength of 325 nm. This is well above the band gap value of CdS. The PL emission at 527 nm is due to the band edge transition. This can also be confirmed from the band gap calculations made from UV-visible absorption studies. The emission at 542 and 572 nm can be attributed to the surface defects/trap states present due to the S, Cd vacancy or Cd interstitials. Blue and green colored high level transitions have been observed at 360, 424 and 443 nm. The luminescence intensity of the entire spectra has increased on adding Ag as the dopant, however the intensity is maximum for sample Ag1, and it decreases on further increase in the concentration of Ag. No silver related surface plasmonics have been observed. This is clear from the XRD patterns also that Ag ions have not replaced the Cd in the CdS matrix; rather there is formation of crystalline silver oxalate. However, these samples may be harnessed to study the anti microbial properties due to the effect of Ag, as well as luminescent detection of the bacteria due to CdS matrix.

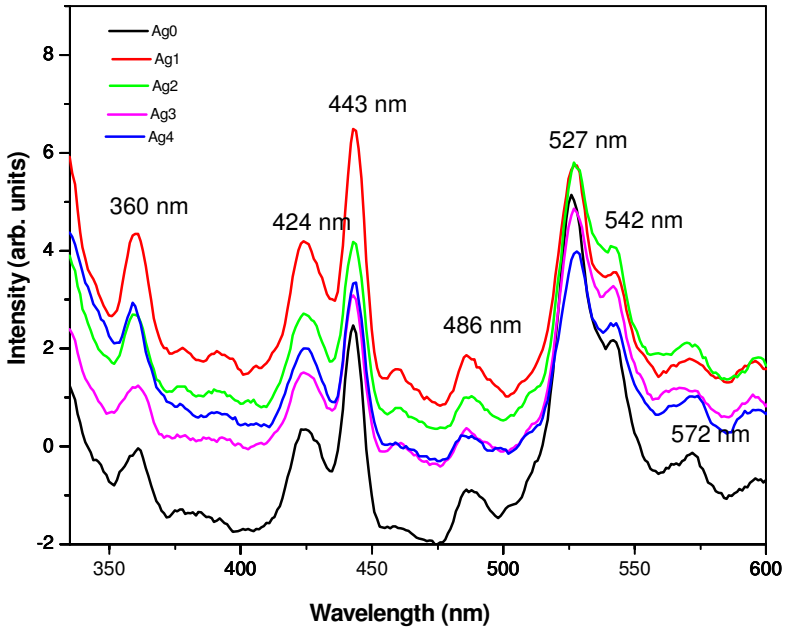

Figure 4.7: PL spectra of CdS/SiO_2 core/shell nanoparticles, undoped and doped with silver, using the excitation wavelength of 325 nm

CHAPTER 5

CONCLUSIONS

Conclusion

The aim of the present work was to synthesize CdS/SiO_2 nanoparticles doped with silver, using sol-gel technique and to characterize them structurally and optically. The work has been concluded as follows:

- CdS/SiO_2 core/shell nanoparticles are found to have hexagonal (wurtzite) structure of CdS along with crystalline silver oxalate phase in the Ag doped nanoparticles. The crystallite sizes of the three samples Ag0, Ag2, and Ag4 have been calculated using Debye Scherrer's formula as 23.65, 52.46 and 44.70 nm respectively. This shows that crystallite size has increased on doping the nanoparticles with silver
- The elemental analysis of sample Ag3, carried out by EDAX, shows that the sample is composed of. Cd (46.41%), S (50.37%) and Ag (3.22%). Thus, Ag atoms have successfully replaced their Cd counterparts as dopant.

- FTIR studies indicate the SiO_2 layer formation on the surface of CdS nanoparticles.

- The band gap of the nanoparticles has been calculated from the differential minima of the absorbance curve. The band gap values of the CdS/SiO_2 nanoparticles are less than that of the bulk value of 2.42 eV.

- No appreciable broadening or shift in the absorption band suggests that the interaction of the silver metal atoms with the CdS is weak, and no surface plasmonic effects emerged on silver doping. Higher concentrations of the Ag should be tried to study the effects more prominently.

- The room temperature PL spectra, at an excitation wavelength of 325 nm, shows an emission at 527 nm, which is due to the band edge transition. The emission at 542 and 572 nm can be attributed to the surface defects/trap states present due to the S, Cd vacancy or Cd interstitials. Blue and green colored high level transitions have been observed at 360, 424 and 443 nm. The luminescence intensity of the entire spectra has increased on adding Ag as the dopant.

References

[1] Quantum Confinement VI: Nanostructured Materials and Devices: Proceedings of the International Symposium *by M. Cahay, Electrochemical Society Staff.*

[2] H. Haug and S. W. Koch**,** Quantum theory of the optical and electronic properties of semiconductors, World Scientific Publishing Co. Pte. Ltd: London, **1990**, 333.

[3] A. P. Alivisatos*, J. Phys. Chem*. **1996**, 100, 13226.

References

[4] M. Nirmal, L. Brus, *Acc. Chem. Res*. **1999**, 32, p. 407.

[5] Kentaro Iwasaki, Prof. Tsukasa Torimoto, , Prof. Tamaki Shibayama, , Dr. Tomohiro Nishikawa, , Prof. Bunsho Ohtani,

[6] Robert Kennedy, Ignacio Martini, Gerg Hartland and Prashant V. Kamat, *Proc. Indian Acad. Sci. (Chem. Sci.)*, **1997**, 109, p. 497-507.

[7] K. Aslan, M. Wu, J. R. Lakowicz, C. D. Geddes, *J. Fluoresc.* March **2007**

[8] L. Viger Mathieu, S. Live Ludovic , D. Therrien Olivier, Denis Boudreau, *Plasmonics* **2008**, 3, p. 33–40

[9] F. Teng, Z. Tian, G. Xiong and Z. Xu, *Catalysis Today,* **2004**, 93-95, p. 651-657

[10] Z. Wang, J. Chen, X. Xue and Y. Hu, *Materials Research Bulletin* **2007**, 42, p. 2211-2218

[11] L. Yao, G. Xu, X. Yang and Y. Luan, *Colloids and Surfaces A: Physicochemical and Engineering Aspects*, **2009**, 333, p. 1-6

[12] J. Chen, Y. M. Zhou, Q. L. Nan, X. Y. Ye, Y. Q. Sun, Z. Q. Wang and S. M. Zhang, *Applied Surface Science*, **2008**, 255, p. 2244-2250

[13] K. Battisha Fizika A **2002** , 11 , p. 61-70

[14] H. T. Xue and P. Q. Zhao, *J. Phys. D: Appl. Phys.* **2009**, 015402, p. 42

[15] D. V. Talapin, A. L. Rogach, A. Konowski, M. Haase, H. Weller*, Nano Lett.* **2001**, 1, p. 207.

[16] I. Mekis, D. V. Talapin, A. Konowski, M. Haase, H. Weller, *J. Phys. Chem.* B **2003**, 107, p. 7454.

[17] X. Peng, M. C. Schlamp, A. V. Kadavanich, A. P. Alivisatos, *J. Am. Chem. Soc.* **1997**, 119, p. 7019.

[18] B. O. Dabbousi, J. Rodriguez-Viejo, F. V. Mikulec, J. R. Heine, H. Mattoussi, R. Ober, K. F. Jensen, M. G. Bawendi, *J. Phys. Chem. B* **1997**, 101, p. 9463.

[19] H. C. Youn, S. Baral, J. H. Fendler, *J. Phys. Chem.* **1998**, 92, p. 6320.

[20] T. Hirai, S. Shijori, I. Komasawa, *J. Chem. Eng. Jpn.* **1994**, 27, p. 590.

[21] A. R. Loukanov, C. D. Dushkin, K. I. Papazova, A. V. Kirov, M. V. Abrashev, E. Adachi, **2004**, 245, p. 9.

[22] L. Qi, J. Ma, H. Cheng, Z. Zhao, *Colloids Surf., A.* **1996**, 111, p. 195.

[23] H. S. Zhou, I. Honma, H. Komiyama, J. W. Haus, *J. Phys. Chem.* **1993**, 97, p. 895.

[24] A. Hasselbarth, A. Eychmuller, R. Eichberger, M. Giersig, A. Mews, H. Weller, *J. Phys. Chem.* **1993**, 97, p. 5333.

[25] G. Hota, S. Jain, K. C. Khilar, *Colloids Surf., A*. **2004**, 232, p. 119.

[26] M. Y. Han, W. Huang, C. H. Chew, L. M. Gan, X. J. Zhang, W. Ji, *J. Phys. Chem.* B **1998**, 102, p. 1884.

[28] E. Wiberg and A. F. Holleman, Inorganic Chemistry, Elsevier **2001**.

[29] R. J. Traill and R. W. Boyle, *American Mineralogist*, **1955,** 40, p. 555.

[30] Charles Kittel, *Introduction to Solid State Physics*, **1995,** 7.

[31] N. Greenwood, A. Norman, Earnshaw, *Chemistry of the Elements*, Oxford: Butterworth-Heinemann, **1997**, 2.

[32] U. Pal, R. Silva-González, G. Martínez-Montes, M. Gracia-Jiménez, M.A. Vidal and Sh. Torres, *Thin Solid Films*, **1997,** 345

[33] P. H. P Wanrooij, U. S Agarwal, J. Meuldijk, J. M. N Kasteren and P. J Lemstra, *Journal of Applied Polymer Science*. 2**,** 1024.

[34] G.H Bogush and C.F Zukoski, J. *Colloid Interface Sci*. **1992,** 19, p. 142.

[35] M. Schiavello, *Fundamentals and Developments Springer*, **1985**

[36] A. Luque, S. Hegedus, *Handbook of Photovoltaic Science and Engineering*, **2003.**

[37] D. C. Reynolds, G. Leies, L. L. Antes and R. E. Marburger, *Phys. Rev***., 1954**, 2**,** p. 533.

[38] U. Kreibig, M. Vollmer, J. P. Toennies, *Optical Properties of Metal Clusters*; Springer-Verlag: Berlin, 1995.

[39] S. Link, M. E. Sayed, A. *Int. Re*V. *Phys. Chem.* **2000**, *19*, p. 409.

[40] J. Yguerabide, E. Yguerabide, E. *Anal. Biochem*. **1998**, *262*, p. 137.

[41] J. Yguerabide, E. Yguerabide, E. *Anal. Biochem.* **1998**, *262*, 157.

[42] H. S. Nalwa, Ed. *Nanostructured materials and nanotechnology*; Academic Press: New York, 2000.

[43] G. Timp, *Nanotechnology*; Springer-Verlag: New York, 1999.

[44] N. Stich, A. Gandhum, Matushin, J. V. Raats, C. Mayer, Y. Alguel, T. Schalkhammer, *J. Nanosci. Nanotechnol.* **2002***, 2* (3/4), p. 375.

[45] N. Stich, A. Gandhum, V. Matushin, C. Mayer, G. Bauer, T. Schalkhammer, *J. Nanosci. Nanotechnol.* **2001**, *1* (1), p. 397.

[46] J. J. Storhoff, R. Elghanian, R. C. Mucic, C. A. Mirkin, R. L. Letsinger, *J. Am. Chem. Soc*. **1998**, *120*, p. 1959.

[47] J. R. Lakowicz, *Anal. Biochem.* **2001**, *298*, p. 1-24.

[48] J. R. Lakowicz, Y. Shen, S. D'Auria, J. Malicka, J. Fang, Z. Gryczynski, *Anal. Biochem.* **2002**, *301*, p. 261.

[49] L. A. Peyser, A. E. Vinson, A. P. Bartko, R. M. Dickson, *Science* **2001**, *291*, p. 103.

[50] L. A. Peyser, T. H. Lee, R. M. Dickson, *J. Phys. Chem. B* **2002**, *106*, p. 7725.

[51] G. H. Bogush, C. F. Zukoski, *J. Colloid Interface Sci.* **1991***,* 142, p. 19.

[52] A.P Philipse, *Colloid Polym. Sci.,* **1988,** 266, p. 1174.

[53] A. V. Blaaderen, J. V. Geest and A. Vrij, *J. Colloid Interface Sci*., **1992,** 154, p**.** 481.

[54] R. Davies, G.A.Schurr, P.Meenan, R.D. Nelson, H.E. Bergna, C.A.S. Bervett and R.H.Goldbaum, *Adv. Mater*., **1998,** 10, p. 1264.

[55] Liz-Marzan, M.Giersig and P.Mulvaney, *Langmuir*, **1996**, 12, p. 4329.

[56] C.H.M. Hofman-Caris, *New. J. Chem*., **1994,** 18, p. 1087.

[57] M. Nirmal, L. Brus, *Acc. Chem. Res*. **1999**, 32, p. 407.

[58] H. Weller, Angew. *Chem. Int. Engl*. **1993**, 32, p. 41.

[59] G. P. Mitchell, C. A. Mirkin, R. L. Letsinger, *J . Am. Chem. Soc*. **1999**, 121, p. 8122.

[60] N. Tessler, V. Medvedev, M. Kazes, S. Kan, U. Banin, *Science* **2002**, 295, p. 1506.

[61] V. L. Colvin, M. C. Schlamp, A. P. Alivisatos, *Nature* **1994**, 370, p. 354.

[62] B. O. Dabboussi, M. G. Bawendi, , O. Onitsuka, and M. F. Rubner, *Appl. Phys. Lett.* **1995**, 66, p. 1316.

[63] M. C. Schlamp, X. G. Peng, A. P. Alivisatos, *Appl. Phys*. **1997**, 82, p. 5837.

[64] H. Mattoussi, L. H. Radzilowski, B.O. Dabbousi, E. L. Thomas, M. G. Bawendi, M. F. Rubner, *j Appl. Phys.* **1998**, 83, p. 7965.

[65] M. Kuno, J. K. Lee, B.O. Dabbousi, F. V. Mikulec, M. G. Bawendi, *J. Chem. Phys.* **1997,** 106, p. 9869.

[66] A. Mews, A. Eychmuller, M. Giersig, D. Schoos, H. Weller, *J. Phys. Chem*. **1994,** 98, p. 934.

[67] M. A. Hines, P. J. Guyot-Sionnest, *J. Phys. Chem*. **1996**, 100, p. 468.

[68] X. Peng, M. C. Schlamp, A. V. Kadavanich, A. P. Alivisatos, *J. Am. Chem. Soc.* **1997,** 119, p. 7019.

[69] B.O. Dabbousi, J. Rodriguez-Viejo, F. V. Mikulec, J. R. Hiene, H. Mattoussi, R. Ober, K.F. Jensen, M .G. Bawendi, *J Phys. Chem*. B **1997**, 101, p. 9463.

[70] D. V. Talapin, A. L. Rogach, A. Kornowski, M. Hasse, H. Weller, *Nano Lett*. **2001**, 1, p. 207.

[71] M. T. Harrison, S. V. Kershaw, A. L. Rogach, A. Kornowski, A. Eychmuller, H. Weller, *Adv. Mater***. *2000*,** 12, p. 123.

[72] G. Allan, G. Bastard, N. Bocara, M. Lanoo, M. Voos, (Eds.) *Heterojunctions and Semiconductor Superlattices,* Springer: Berlin Heidleberg **1986.**

[73] L.L.Hench and J.K.West, The Sol-Gel Process Chem. Rev., **1990,** 33, p. 90.

[74] C.B. Murray, D. J. Norris, M. G. Bawendi, *J. Am. Chem. Soc.* 1993, 115, p. 8706.

[75] X. Peng, J. Wickham, A. P. Alivisatos, *J. Am. Chem. Soc*. **1998**, 120, p. 5343.

[76] A. L. Smith, *Particle Growth in Suspensions*; Academic Press: London, 1983.

[77] J. E. B. Katari, V. L. Colvin, A. P. Alivisatos, *J. Phys. Chem*. **1994**, 98, p. 4109.

[78] (a) D. L. Klein, R. Roth, A. K. L. Lim, A. P. Alivisatos, P. L. McEuen, *Nature* **1997**, 389, p. 699; (b) D. L. Klein, et al. *Appl. Phys. Lett*. **1996**, 68, p. 2574.

[79] C. J. Loweth, W. B. Caldwell, X. G. Peng, A. P. Alivisatos, P. G. Schultz, *Angew. Chem. Int. Ed. Engl*. **1999**, 38, p. 1812.

[80] M. Kuno, J. K. Lee, B. O. Dabbousi, F. V. Mikulec, M. G. Bawendi, *J. Chem.. Phys***. 1997**, 106, p. 9869.

[81] M. Jacobsohn- Ellon, T. Mokari, U. Banin, *J. Phys. Chem*. *B* **2001**, 105, p. 12726-12731.

[82] S. Thomas, D. Sakthikumar, P. A. Joy, Y. Yoshida and Anantharaman M R **2006** Nanotechnology 17 5565.
[83] Robert M. Silverstein, Francis X. Webster, Spectrometric Identefication of Organic Compounds, sixth edition, p. 108.